ULTRAVIOLET COMMUNICATIONS FOR AIRBORNE LINKS

A Thesis

by

Hamed Tadayyoniahrab

Submitted to the

Graduate School of Sciences and Engineering
In Partial Fulfillment of the Requirements for
the Degree of

Master of Science

in the
Department of Electrical and Electronics Engineering

Özyeğin University
July 2019

ULTRAVIOLET COMMUNICATIONS FOR AIRBORNE LINKS

Approved by:

Professor M. Uysal, Advisor,
Department of Electrical and
Electronics Engineering
Özyeğin University

Assisstant Professor K. Durak
Department of Electrical and
Electronics Engineering
Özyeğin University

Assistant Professor B. Karakaya,
Department of Electrical and
Electronics Engineering
Istanbul University

To the one love who always supported me

and

my beloved parents

ABSTRACT

Ultraviolet (UV) communication enables non-line-of-sight (NLOS) wireless connectivity through strong molecular and aerosol scattering. Due to their NLOS nature, UV links bring robustness to blockage or shadowing and relax the pointing, acquisition and tracking requirements. This feature is particularly appealing for unmanned aerial vehicle (UAV) networks. In this work, we consider the uplink of a ground sensor network where a number of sensor nodes are placed on the ground in a serial manner and with equal intra-distances. A UAV periodically visits the area and collects the sensor data from ground nodes. For the uplink transmission under consideration, we investigate the performance of UV-based system and determine the maximum UAV coverage to maintain a pre-defined bit error rate performance.

In the first chapter, we bring an overview of ultraviolet communications. We study the advantages of UV communications in addition to its disadvantages. Finally we mention our motivations for this work, based on the mentioned UV communication features and their comparison to other communication media (including radio frequency and other optical wireless communications technologies).

In the second chapter, we provide UV channel modeling for airborne links, considering different possible geometric configurations in the ground-to-air links.

In chapter three, we study a UV-based ground-to-air link system, considering the uplink of a ground sensor network, for which an unmanned aerial vehicle (UAV) periodically

visits the network of serially-placed sensors and collects the sensor data from ground nodes. We analyze the system performance and find the maximum UAV coverage to maintain a pre-defined bit error rate (BER) performance.

In chapter four, we study the uplink of ground sensor network, with a UAV-based receiver, considering the interference from the other sensor nodes, while an intended node is communicating with the receiver. We analyze the system by providing bit error rate performance for such a scenario.

Finally in chapter five we conclude our discussion on UV communications for airborne links.

ÖZET

Morötesi (Ultraviolet - UV) güçlü molekül bağı ve aerosol saçılması ile bire bir görmeden çalışmayı(non-line-of-sight - NLOS) mümkün kılar. NLOS doğasından ötürü UV linkleri tıkanıklığı veya gölgeyi sağlamlaştırır ve doğrultuyu, kazancı ve takip gerekliliklerini rahatlatır. Bu özellikle İnsansız Hava Aracı (unmanned aerial vehicle - UAV) ağlarında iş görür. Bu çalışmamızda sensor node'larının yeryüzüne seri ve eşit intra mesafelerle yerleştirilmiş ground sensor network ‘unun uydu bağlantısı üzerinde çalıstık. Çalışmamızda bir UAV periyodik bir şekilde alanı ziyaret edip yer nodlarindan sensör verisi topladı, uydu verilerini de göz önünde bulundurarak UV bazlı sistemin performansını ölçtük ve maksimum UAV coverage'ini belirli bir bit error rate performansıyla hesapladık.

İlk bölümde ultraviyole communication'a değindik ver artı-eksilerinden bahsettik. Son olarak UV communication özelliklerine ve diğer medya karşılaştırmalarına da değinerek bu çalışmadaki motivasyonlarımızdan bahsettik.

İkinci bölümde ground to air linklerdeki çeşitli geometrik konfigürasyonlar ile birlikte airborne linkler için UV channel modelinden bahsettik.

Üçüncü bölümde UV bazlı ground to air link sistemi üzerinde çalıştık. Uydu verilerini de göze alarak bir İnsansız Hava Aracı (UAV) periyodik şekilde seri yerleştirilmiş sensörleri ziyaret etmesini üzerine değindik ve maksimum UAV coverage'ini belirli bit error rate (BER) ile belirledik.

Dördüncü bölümde sensörün uydu verisinden bahsettik, diğer node’larin da etkileşimini göz önünde bulundurarak hedeflenen node'un alıcıyla bağlantı kurması üzerinde çalıstık. Bu senaryoda sistemi bit error performance'i sağlayarak analiz ettik

Son olarak beşinci bölümde airborne linkler için UV communication çalışmamızı özetledik.

ACKNOWLEDGMENTS

I would like to express my deepest gratitude and sincere appreciation to my supervisor, Prof. Dr. Murat Uysal for the patience, guidance and time that he has provided for me. I would like to thank him for the support, motivation and immense knowledge that he has provided for me throughout my studies. Also, I have to thank the jury members, whom helped enriching this thesis, by their valuable comments.

This work was supported by the Turkish Scientific and Research Council under Grant 215E311. The statements made herein are solely the responsibility of the authors.

TABLE OF CONTENTS

LIST OF TABLES

LIST OF FIGURES

CHAPTER I

INTRODUCTION

Optical Wireless Communication (OWC) refers to the communication techniques and technologies which enable establishing connection between the transmitter and the receiver by using electromagnetic waves within the wavelengths which are considered as part of the optical range. The wavelengths which are among the optical range are infrared (IR), visible light (VL) and ultraviolet (UV). There are many advantages in using optical wireless communications, which will be mentioned briefly in the beginning of this chapter. Some applications of optical wireless communications include using them as a substitute to the current communication techniques and technologies (mostly radio frequency (RF) communications) and some of them include using them as complementary to the current technologies (for example when the existing wireless technologies are not available due to some air conditions or when the bandwidth and speed which they provide is not satisfactory for that application). In addition to the general advantages of the optical wireless communications, ultraviolet communication has some additional interesting features which are advantageous enough to enforce using it for certain applications, where the other two optical wireless communication technologies are less useful.

In this chapter, we first briefly introduce the optical wireless communications in addition to some of their features and advantages which are the motivation to use them. Then we go through UV communication, its history and its special features which gives us strong intent to use it in certain applications, including the one in this work. Then we go through

literature, to see what has been done in this area and mention some research gaps. Finally, we introduce the special application which we are considering for UV communications in this work and we present our motivations according to the research gap which we have already mentioned.

1.1 Optical Wireless Communications

Wireless communications have already changed our lives by the tools which gives to us. Those tools are working based on the related wireless technologies. While the use of wireless technologies is life-changing for the time being, the foreseen applications of those technologies anticipate that the use of the current technologies may not be satisfying in the near future, due to some upcoming problems. One of those problems is that the bandwidth that the current technology is providing, sometimes may seem not adequate even for the current applications, let alone the future demands. One way to overcome such a problem is using theories and techniques which enables the use of the provided bandwidth in a more efficient way. Even by using those new complicated methods and techniques, still the demand for bandwidth is increasing and that encourages us to look for other parts of the electromagnetic spectrum and try to use the parts which has not been considered to have communication usage before [1]. The other motivation for looking for ways to use the other parts of the electromagnetic spectrum is that the use of radio frequency part of the spectrum is regulated and most of the RF bandwidth is occupied and utilized by different applications and thus there is not much bandwidth remained to be used for the new upcoming applications, and even in case there is some bandwidth, using it will be expensive. Therefore, making use of the upper band of the electromagnetic spectrum, not only promises a usage which is unregulated, but also is free-to-use and therefore there is no restriction in utilizing that part

of the spectrum for the new applications and technologies. There are other advantages in using optical wireless communications over the radio frequency communications, which include robustness to electromagnetic interference, high degree of spatial confinement which leads to unlimited reuse of spectrum and physical security [2].

1.2 Ultraviolet Communications

The interest on ultraviolet communications has been growing in the recent years. One of the reasons for this growing interest is the recent advances in the solid-state optical sources and detectors [1] that are used in the communication-appropriate band of UV.

In addition to the reason which was introduced above, there are other reasons for the growing interest for the research in the area of UV communications, some of which are the advantages that ultraviolet communications may have over other types of optical wireless communications (i.e. visible light communications and free space optical communications (FSO)) in some applications and will be mentioned through the following.

As seen in Fig.1, ultraviolet band is considered to start in 100 nm and end around 400 nm in the electromagnetic spectrum. UV band itself is divided into three sub-bands including UVA (315-400 nm), UVB (280-315 nm) and UVC (100-280 nm). The reason that these bands are distinguished is that the UV absorption of different layers of the earth atmosphere from the sunlight is different for each sub-band and therefore, some features of the sub-bands (including the background noise which is imposed by the solar radiation on the systems which operate in that band) are different. This difference results in UV-C band to be the main interest in UV communications [3]. The reason is that UV-C sub-band is solar-blind, i.e. the solar UV rays within that sub-band cannot enter the earth atmosphere and are absorbed by

the ozone layer, therefore enabling the communication link which is utilizing the UV-C sub-band at the ground level not to be affected by the solar rays. This results in for the effect of the background noise to be negligible. UV-C band is also called deep UV band.

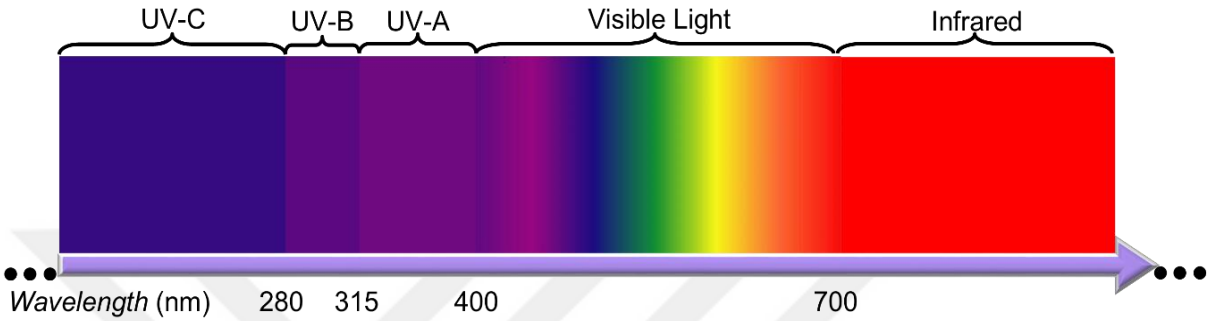

Figure 1: Optical Range of Electromagnetic Waves

The main feature that can be mentioned for the ultraviolet communications is that due to the high amount of atmospheric scattering for the waves in the UV-C band, non-line-of-sight (NLOS) connectivity is enabled between the source and the detector [4, Ch.8].

1.2.1 UV Communications History

The first studies on ultraviolet technology for the purpose of communications date back to the 1960s, where it was considered to be used for naval applications [5]. One of the first experiments was performed in MIT in 1968 and targeted characterizing the ultraviolet communication link over a range of more than 20 kilometers [6]. In that experiment, xenon flashtube was used as the transmitter, radiating waves with minimum wavelength of 280 nm and a photomultiplier tube (PMT) was used as the receiver.

It was around the time that Reily published his famous thesis concerning the ultraviolet communications temporal channel model [7]. after that an NLOS UV system

based on isotropic radiating mercury arc lamp was demonstrated [8]. The primary modulation rate for this experiment was only 40 kHz. This modulation rate was improved to 400 kHz by the use of a mercury-xenon lamp to cover a range of 1 km [9]. To avoid the background noise, this experiment was performed in wavelength of 265 nm. A few years later, some experiments were performed in wavelength of 266 nm, with rate of few hundreds of meters [10].

Primarily, for the first decades, UV communication studies were handled by using one of the following as the receiver: either flashtubes or lamps or lasers [11]. All of these were massive, not power-efficient and as it was stated above, could operate in a limited bandwidth. This made the first generation of UV transceivers not suitable to be used in applications such as UAV communications. These days, on the other hand, the new semiconductor UV transmitters cost less, have higher reliability, consume less power and operate in a much higher bandwidth. Some companies have commercialized UV LEDs and so the prices have already dropped a lot, making the UV communication promising to be used in the areas such as ground sensor networks and UAV communications. Other advantages of the new technology which makes the UV communications suitable for civilian applications is that the new UV LEDs radiate optical power in the order of a fraction of a mW, which is much less than the previous technologies and more proper for the human health, in case of direct contact.

1.2.2 UV Transmitter and Receiver Technology

The technology which is used in the UV receivers has also improved significantly in the recent years. The two types of photodetectors which are used as receivers are photo

multiplier tubes (PMTs) and avalanche photo diodes (APDs). The problem with PMTs is that they are a little bulky, fragile, expensive and power consuming at the time. Their advantage is that they have large effective area and large multiplication gain of 10^5~10^7 or more. Also, because they are resistive to background noise (due to small dark current), they are very suitable for detecting weak signals, which are very likely in the ultraviolet communications. On the other hand, for avalanche photodiodes, one of the good examples of the commercialized APDs is silicon carbide (SiC) APD, which has a good gain of 10^5~10^6 with an acceptable sensitivity [12].

1.2.3 UV Communication applications

According to the recent advances in the ultraviolet transmitters and receivers hardware, UV communication is now desired in some civilian applications as well as the military ones. One of the potential civilian applications is distributed sensor network [13]. Some potential military applications are unattended ground sensor networks [14], communications between the small units [14], and covert networking [11].

On the other hand, some disadvantages may restrict the usage of ultraviolet communications for civilian applications. One of those disadvantages is the limits for which human eye and skin should avoid being under UV exposure. Those limits are taken care of by some international organizations such as International Electrotechnical Commission and International Commission on Non-Ionizing Radiation Protection [15]. That is one of the design restrictions which should be kept in mind while designing the UV communication systems. This restriction should be considered in a way that the amount of time for which a

human being may be in contact with the UV radiation is maintained for a certain amount of UV energy per square centimeters.

1.2.4 UV Communications Advantages over Infrared Communications

In addition to the mentioned features for optical wireless communications, ultraviolet communication introduces some other interesting advantages even over the other optical wireless communication technologies.

One of the advantages that ultraviolet communication has over infrared communication is that due to the solar-blindness of the communication in the UVC band, the usage of wild field-of-view detectors as the receivers is possible. This feature is especially beneficial in outdoor usage of ultraviolet communications as it significantly improves the amount of energy that can be gathered by the ultraviolet receivers. For the free space optical communication this is not the case.

The other advantage of ultraviolet communication over free space optical communication is that the FSO communication is a point-to-point type of communication, which requires a high accuracy of pointing between the source and the detector. Therefore, to use the free space optical communication, pointing, acquisition and tracking (PAT) is required. On the other hand, ultraviolet communication, as mentioned before, enables non-line-of-sight communications and therefore the requirement for using the PAT is eliminated or at least relaxed.

The combination of these advantages results in the ultraviolet communication to be used in outdoor cases where either the conventional radio frequency infrastructure or free space optical links are unavailable or unreliable [16].

1.3 Ultraviolet Communications for Airborne Links

The two features which were mentioned previously are our motivations in this work. Firstly, as mentioned above, Ultraviolet communication enables non-line-of-sight wireless connectivity through strong molecular and aerosol scattering. Due to their NLOS nature, UV links bring robustness to blockage or shadowing and relax the pointing, acquisition and tracking requirements. Secondly, because of the possibility of the use of wide field-of-view receivers as the detectors, due to the negligible background noise in the deep UV band, the energy scattered from molecular and aerosol particles within the common volume between transmitter and receiver cones can be efficiently captured by such receivers. Moreover, due to the wide field of view property of the receivers, the UV transceivers are able to maintain connectivity better while one of the transmitter or the receiver or both are moving [17]. These two features are particularly appealing for unmanned aerial vehicle (UAV) networks. Through the following lines, we address the research gap regarding this issue, as the motivation of this work.

1.4 Literature Review

There is already a growing literature on UV communication that covers a wide range of topics on channel modelling, physical layer design and upper layer design issues. Modeling the UV propagation based on single scattering was first studied studied in [18] and [19]. After that, a significant effort has been made to model the UV channel in various deployment scenarios, including investigation of different methods for finding exact channel impulse responses in coplanar non-line-of-sight configurations [20, 21]. Coplanar configurations are the ones in which the transmitter and receiver cone axes are in the same

plane. In order to extend the model to comply with more generic cases where transmitter and receiver cones are not in the same plane, [22, 23] has proposed a general model for non-coplanar cases (which of course is in agreement with the previously proposed coplanar models in particular conditions).

As most of the work on ultraviolet channel modeling consists of finding an integral form for the channel impulse response and the channel geometric path loss, there has also been efforts to find approximate closed form for the channel path loss of the non-line-of-sight configuration as in [24- 26]. The other efforts to find a channel path loss for the ultraviolet communication through experimental work in [27], where a very simple path loss is proposed and confirmed by experiment.

Most of these works build upon the assumption on single scattering while some sporadic works address multiple scattering [28- 30]. Earlier works on UV have mainly considered single-carrier systems [15,16] where simple pulse modulation techniques are used. More recent works have explored advanced concepts such as multi-carrier communication [31], multiple-input multiple-output (MIMO) techniques [32] and relay-assisted transmission [31, 33] to enable long-range and high-speed UV links. Upper layer design issues such as connectivity in networks were further explored in [34- 36]. In [35], the authors focus on applying the fundamentals of connectivity on an ultraviolet network, considering the simple channel provided by [32], just to observe the connectivity properties of the ultraviolet network while employing the simple path loss model of [32] for an all upward-looking UV transceiver nodes. In [34], the same approach is taken, but this time, the fact that all the transceivers in the network may not be looking upwards is taken into account, while using the same simple path loss model which was used in the previous work. In [36],

the performance of a UV network is investigated through outage metric, by still using the same path loss model from [32].

In recent years, there has been an increasing attention on the use of unmanned aerial vehicles for various military and civilian applications. Free space optical communication systems operating at infrared (IR) wavelengths [37, 38] were proposed as a potential wireless connectivity solution for UAV-to-ground and UAV-to-UAV links. Due to narrow beams of employed IR laser transmitters, FSO links require strict pointing, acquisition and tracking requirements (PAT) for such mobile applications. Due to their NLOS nature, UV links bring robustness to blockage or shadowing and relax the PAT requirements associated with FSO links particularly important for UAV networks.

The current research efforts on UV mainly address terrestrial links and assume that both transmitter and receiver are located on the ground. The concept of great and unique capabilities of ultraviolet communications which makes it perfect to be used in an unattended ground sensor network has been discussed was discussed in [14], while it did not go through the mathematical details and modeling and only addressed the properties which enable UV communication to provide such a great infrastructure for the sensor networks. Some of those features are covertness, jam resistance, energy efficiency, low sensitivity to adverse meteorological conditions, low sensitivity to ground proximity, low sensitivity of the link connections to emplacement modes, ability to operate both in line-of-sight and non-line-of-sight configurations and the ability to provide minimum bit error rate and acceptable data rate for the sensor network-related applications [14]. In that paper, the concept of using UV communications in UAV networks is not addressed.

To the best of our knowledge, UV communication in the context of UAV networks was only investigated in a very recent work [39], where the network connectivity was investigated based on a random waypoint mobility model. In this paper, the channel model in [27] is used. The problem with using that channel model is that it can be used only when all the geometric parameters which affect the geometric path loss are constant and that is achieved only when whether all the nodes in the network are not moving or only flying in the same height, while looking upwards.

1.5 Thesis Structure and Contributions

This thesis is organized as follows: In chapter 2, we consider different possible geometric scenarios for the ultraviolet communication used for UAV communications. We provide the channel model for each of the scenarios and compare the models to show their differences and similarities and emphasis on the significance of differentiating them.

In chapter 3, we consider the uplink of an unattended ground sensor network, using a proper channel model which depicts the geometrical parameters changes for different possible scenarios, where a number of sensor nodes are placed on the ground in a serial manner and with equal intra-distances. A UAV periodically visits the area and collects the sensor data from ground nodes. The UV receiver on the aerial vehicle is located such that the receiver cone faces the horizontal axis while UV transmitters in ground sensors face upwards. For the uplink transmission under consideration, we investigate the performance of UV-based aerial system and determine the maximum UAV coverage to maintain a pre-defined bit error rate (BER) performance.

In chapter 4, we investigate the presence of interference on the performance of the same system. In that chapter, we consider the uplink of an unattended ground sensor network, while the link to the nearest sensor is considered as the main link and the other UV links is considered as the interference.

Finally, in chapter 5, we present the conclusion of our works.

CHAPTER II

UV CHANNEL MODELING FOR GROUND-TO-AIR LINKS

2.1 Introduction

There has been a comprehensive study for UV channel modeling throughout the literature, especially for the non-line-of-sight (NLOS) configurations. As it was briefly mentioned in the previous chapter, these studies include investigations on finding the comprehensive channel impulse response, finding the approximate closed form for the geometric path loss, obtaining the simple power decay model and its corresponding parameters through experiment, and proving the results of the mentioned models with testbeds and experiments.

The geometric channel in UV communications is strongly dependent on the change of geometric parameters, therefore if we are considering a UAV system in which one of the transmitter or receiver (or both) are carried by a UAV, the changes in the geometric channel have to be studied. There has not yet been a study in which the effect of moving on the UV channel has been shown explicitly, therefore in this chapter we try to manipulate the existing channel models to show the effect of movement.

Here in this chapter, we mention the scenarios in which we are going to study UAV communications through UV links and the proper channel modeling which is suitable for each of the scenarios will be presented in accordance to the point that the channel model

should be able to depict the changes in the channel which are imposed by the movement. It worth mentioning that the assumption for finding the UV channel in this work is single-scattering.

2.2 Channel Modeling for Possible Configurations in UV Ground-to-Air Links

As it will be described throughout the next chapters, the configurations which we will study will include a ground-based transmitter facing upwards and a UAV-based receiver which is located on the UAV and the UAV is moving towards the aforementioned transmitter. For the UAV-based receiver, three different configurations will be considered. The configurations for the receiver are shown in Fig. 2, Configuration A is such that the receiver cone faces the horizontal axis. Configuration B is where the receiver is facing downwards. Finally, configuration C is when the receiver is facing upwards. In this following, for each of the configurations, the proper channel model will be introduced. The introduced channel models will be used throughout the analysis in the next chapters correspondingly for the relevant scenarios.

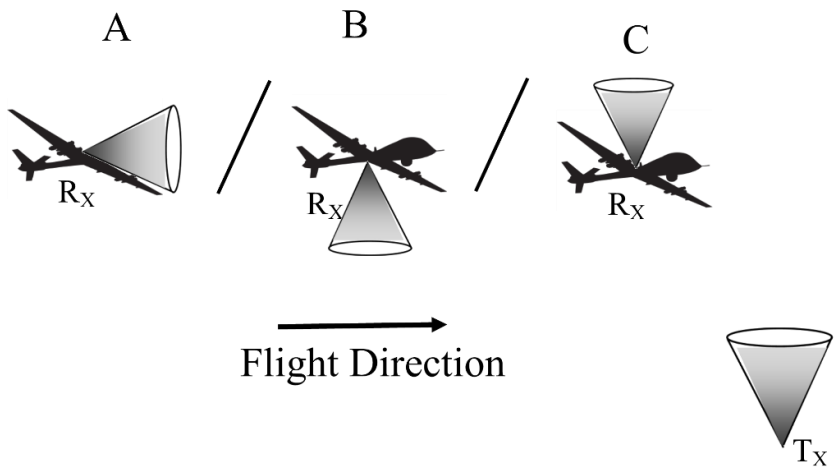

Figure 2: Different possible configurations for ground-to-UAV UV link

2.2.1 Channel Model for Configuration A

The details for the first configuration are shown in Fig.3. The receiver is at the height of d above the ground and the horizontal distance between the transmitter and the receiver is r. The transmitter beam divergence is Θ_T and the receiver field of view (FOV) is Θ_R. As it is seen in the figure, this configuration consists of a non-line-of-sight link between the transmitter and the receiver which enables communication through scattering by the common volume V between the transmitter and receiver cones which is shown in Fig.3. The NLOS path can be modeled as combination of two LOS paths: one from the transmitter to the common volume and the other one from the common volume to the receiver. To obtain the amount of energy transmitted through this link, we consider a random incident point inside the common volume and call it as P. Assume that the angle between a vector pointing from the receiver vertex to the point P and the receiver axis is ζ. Imagine that the distance of P from the transmitter and the receiver is r_1 and r_2 respectively. Assume that an impulse of unit energy is emitted from the transmitter at time $t = 0$ in a uniform manner. The amount of energy received at the point P resulted by the LOS link between the transmitter and that point is

$$E_p = \frac{\exp\left(-k_e r_1\right)}{2\pi\left(1-\cos\frac{\Theta_T}{2}\right)r_1^2} \tag{1}$$

where k_e is the atmospheric extinction factor and the term $2\pi\left(1-\cos\Theta_T/2\right)$ accounts for the transmitter solid cone angle (in steradians). k_e is found by $k_e = k_s + k_a$ in

which k_a is atmospheric absorption coefficient and k_s is the atmospheric scattering factor and can be found as the summation of molecular (Rayleigh) and aerosol (Mie) scattering coefficients denoted by k_s^{Ray} and k_s^{Mie} respectively,

In order to sum up all the received energy at the common volume V, a differential volume ∂V is defined around the incident point of P. This differential volume can now be considered as another source which is emitting energy towards the transmitter. Then, the amount of energy received by the transmitter through the second LOS link is

$$\partial I = \frac{E_P k_s \phi(\Theta_S) \cos\zeta \exp(-k_e r_2) a}{4\pi r_2^2} \partial V \tag{2}$$

in which, a is the receiver effective area, Θ_S is the scattering angle and $\Phi(\Theta_S)$ denotes the scattering phase function which is found by the weighted sum of the Rayleigh and Mie phase functions as

$$\phi(\Theta_s) = \frac{k_s^{Ray}}{k_s} \phi^{Ray}(\Theta_s) + \frac{k_s^{Mie}}{k_s} \phi^{Mie}(\Theta_s) \tag{3}$$

in which

$$\phi^{Ray}(\Theta_s) = \frac{3}{4(1+2c_1)}\left(1+3c_1+(1-c_1)\cos^2\Theta_s\right) \tag{4}$$

$$\phi^{Mie}(\Theta_s) = \frac{1-c_2^2}{\left(1+c_2^2-2c_2\cos(\Theta_s)\right)^{1.5}} + \frac{0.5c_3\left(3\cos^2(\Theta_s)-1\right)\left(1-c_2^2\right)}{\left(1+c_2^2\right)^{1.5}} \tag{5}$$

with $c_1 = 0.017, c_2 = 0.72$ and $c_3 = 0.5$ [9].

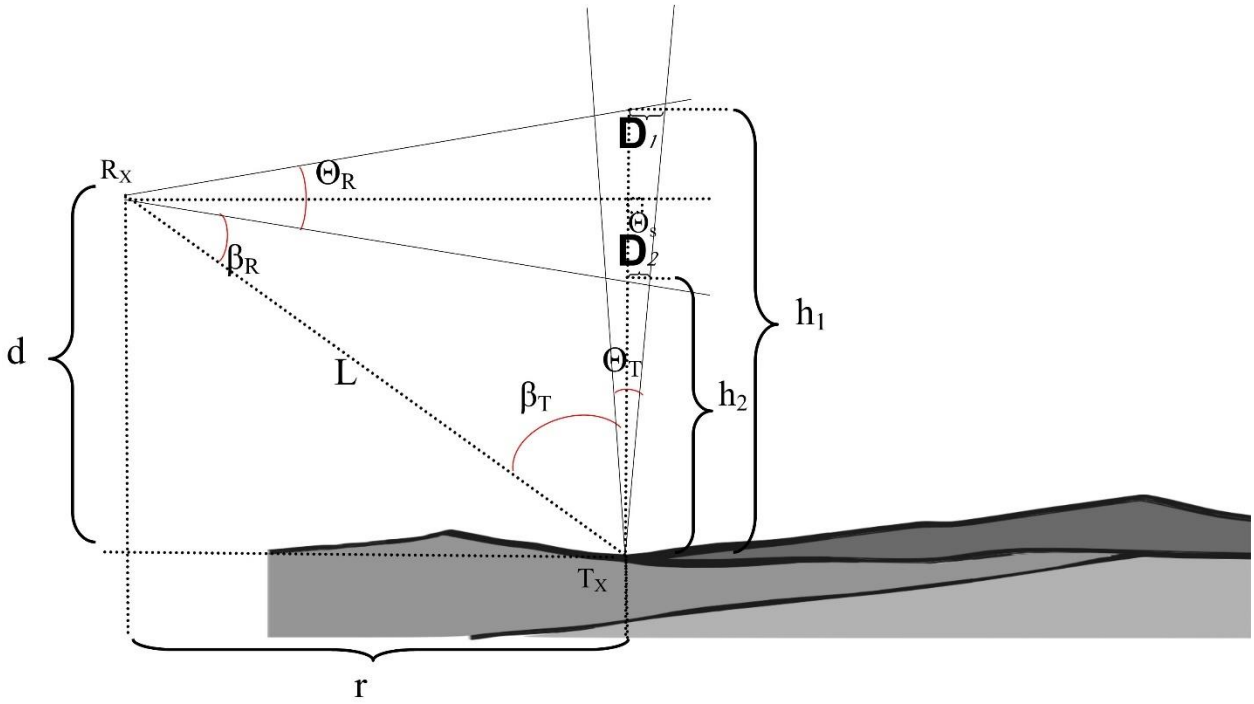

Figure 3: UV link geometrical configuration between ground node (transmitter) and UAV (receiver) in configuration A

The phase function is the probability density function of the scattering angle (Θ_s) and decides the probability of the scattering of a propagating photon [40]. The phase function in (4) follows a generalized Rayleigh model and the phase function in (5) follows a generalized Henyey-Greenstein model [41]. To have a perception of the amount of the generalized phase function in (3) for different scattering angles, Fig. 4 shows the effect of scattering angle on the phase function.

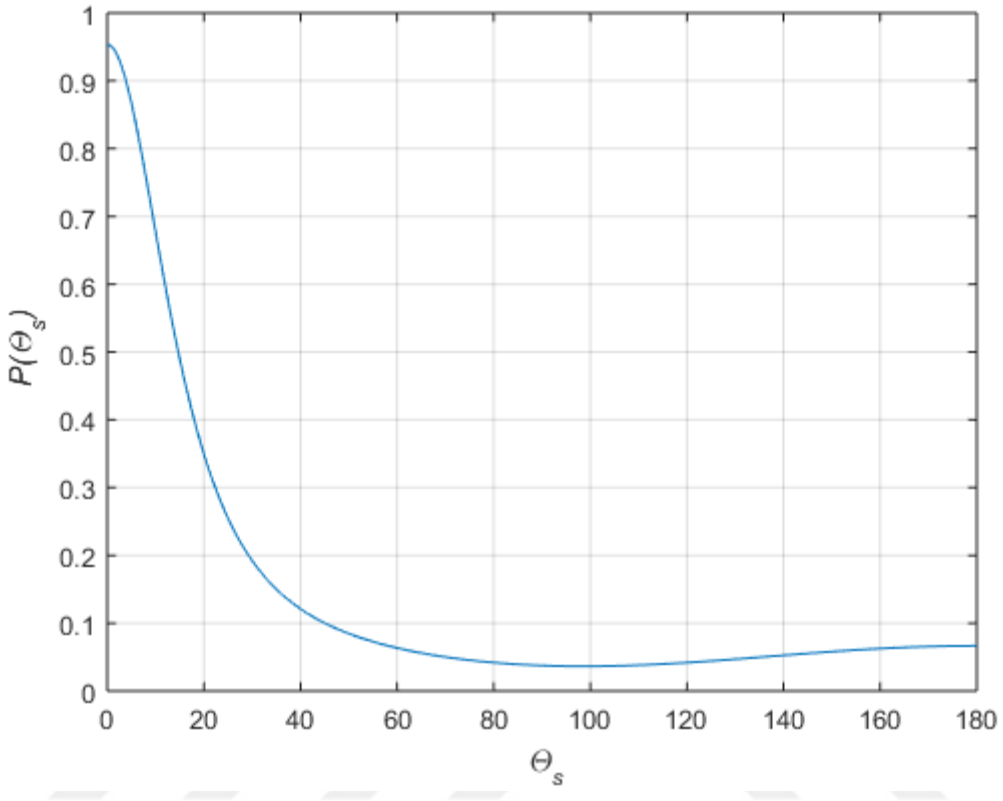

Figure 4: The effect of scattering angle on scattering phase function

It is seen that the scattering angle increases, the weighted sum of the two different phase functions decreases in a meaningful manner. To find the received energy in the receiver, we have to insert (1) into (2) and then integrate the expression over the whole common volume V. One problem is that not only this integration does not have any closed form, but also the integration bounds are variables which are changing for every incident point inside the common volume. Therefore, in order to find a closed form for the received energy, in certain conditions where the transmitter beam divergence is small (as in this work), we assume all the incident points to be approximated as one point which is the intersection of the axes of two cones. In that case $r_1 = d$, $r_2 = r$ and $\zeta = 0$ and $\Theta_s = 90^o$, resulting in

Rayleigh and Mire scattering phase functions in (3) to become $\Phi^{Ray} = 3\left(1+3c_1\right)/4\left(1+2c_1\right)$ and $\Phi^{Mie} = \left(1-c_2^2\right)\left(1-0.5c_3\right)/\left(1+c_2^2\right)^{1.5}$. Also, the common volume can be approximated as a frustum of right angle with the volume of $V = (1/3)\pi(D_1^{\,2}h_1 - D_2^{\,2}h_2)$ where $h_1 = d + r\Theta_R/2$, $h_2 = d - r\Theta_R/2$, $D_1 = h_1\Theta_T/2$ and $D_2 = h_2\Theta_T/2$. Using these parameters, the approximate optical received power (irradiance) at a horizontal distance of r from the transmitter can be calculated as [26]

$$I(r) \simeq \frac{k_s \Phi \exp\left(-k_e\left(r+d\right)\right) aV}{8\pi^2\left(1-\cos\left(\frac{\Theta_T}{2}\right)\right) d^2 r^2} \tag{6}$$

Substituting V in (6), we have

$$I_{configA}(r) = \exp(-k_e r) A\left(\frac{1}{r} + Br\right), \tag{7}$$

where A and B are defined as

$$A = \frac{k_s \exp\left(-k_e d\right) \Phi a \theta_T^2 \theta_R}{32\pi\left(1-\cos\left(\theta_T/2\right)\right)} \tag{8}$$

and

$$B = \frac{\theta_R^2}{12d^2}. \tag{9}$$

The representation of the geometric channel in (7) depicts the effects of movement on the channel in a clear way as all the parameters have been converted to their equivalent in terms of the horizontal distance between the transmitter and the receiver.

2.2.2 Channel Model for Configuration B

To find the channel in the second configuration, we must consider two different possibilities shown in Fig. 5 B1 and B2.

For both possibilities, the parameters of flight, transmitter, receiver, scattering and extinction for this configuration are the same as the previous one. In addition to those parameters, the transmitter and receiver elevation angles are defined as the angle between the transmitter axis and the receiver axis with the transmitter- receiver connecting line and are denoted by β_T and β_R respectively. Also, the separation distance between the transmitter and the receiver is denoted by α . The transmitter and receiver vertices are denoted by T and R respectively and are connected by TR line.

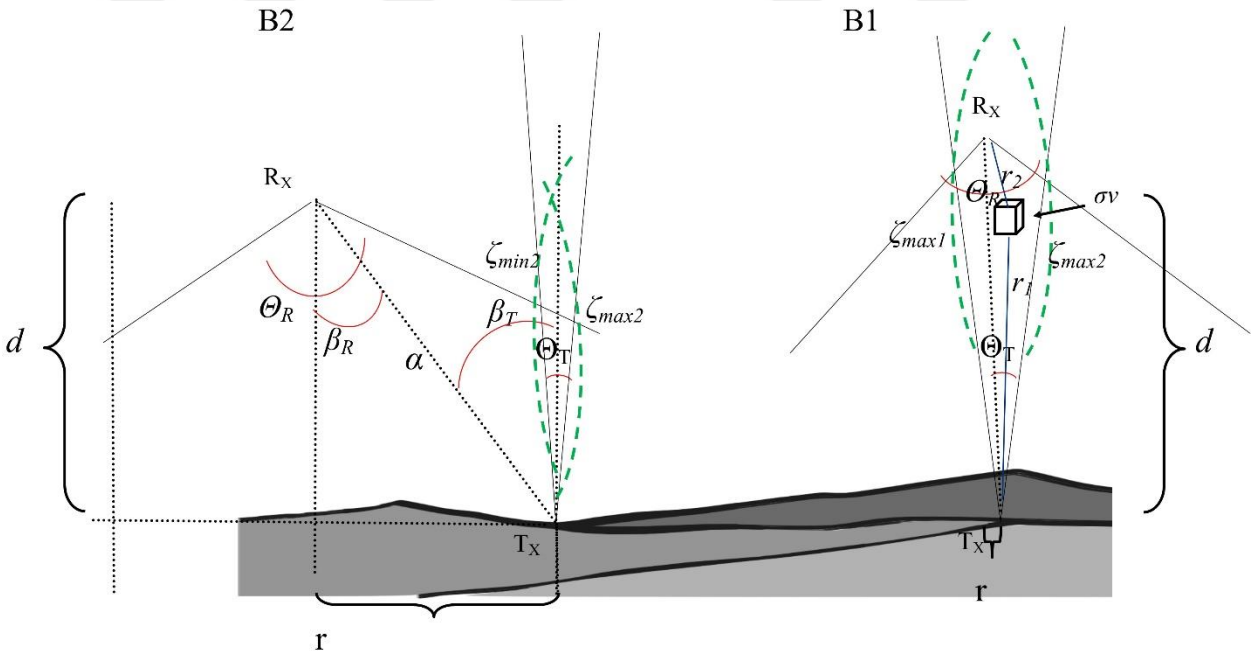

Figure 5: UV link geometrical configuration between ground node (transmitter) and UAV (receiver) in configuration B

For the possibility B1, the approach to find the single-scattering channel is the same as previous case, unless the integral form of the channel cannot be found as a closed form. That is because in this configuration, as it is seen in Fig. 5, the common volume between the transmitter and the receiver is very large, therefore, one cannot approximate all the incident points as one point. This prevents us to find an approximate closed form for the channel in this configuration. Therefore, in order to find the channel in this configuration, we have to define the integral bounds in the integral form of the channel in

$$\partial I = \frac{k_s \phi(\Theta_S)\cos\zeta \exp(-k_e(r_1+r_2))a}{8\pi^2 r_1^2 r_2^2\left(1-\cos\left(\frac{\Theta_T}{2}\right)\right)}\partial V \,. \tag{10}$$

In order to do that, we must first choose a proper coordinate system. Here we consider a prolate-spheroidal coordinates system. Choosing prolate-spheroidal coordinates has the advantage of using the characteristic of a surface of a prolate spheroid, which is: the distance between the foci of the prolate spheroid through any point on its surface is constant. So, if we put the transmitter and receiver on the foci of a prolate spheroidal coordinate system, the summation of the distance of any point on each of the constant prolate spheroid surfaces (denoted by $\xi = cte$) from the two foci will be constant. Thus, all of the points on each prolate spheroidal surface can be characterized by only a constant ξ. This means that if an impulse with unit optical power is transmitted from the Tx located on one of the focal points of the prolate spheroidal coordinates, then the distance (and hence the time) that takes for the impulse to be scattered from all of the points on a single prolate spheroid surface of $\xi = cte$ and reach to the Rx which is located on the other focal point of the coordinate system is the

same. Thus, if we simply sum all the energy scattered from all of the points on one prolate spheroid, then we have one impulse response regarding that $\xi = cte$ and hence regarding the specific time t corresponding to that ξ.

In this coordinate system each point's location is determined by three components of (ξ, η, ϕ) which are called radial, angular and azimuthal coordinates. Consider that we have put our Tx and Rx on the focal points of this coordinate system. Suppose that the differential volume that we are going to use it to sum up all the scattered energy is ∂V which is located r_1 meters far from the transmitter and r_2 meters far from the receiver. The curves of constant $\xi = (r_1 + r_2)/\alpha$ are surfaces of aforementioned prolate spheroids ($\xi \geq 1$). The curves of constant $\eta = (r_1 - r_2)/\alpha$ are surfaces of hyperboloids of revolution ($-1 \leq \eta \leq 1$). Finally, ϕ is the azimuthal angle measured from the x axis in the Cartesian coordinates to the orthogonal projection of the point on the xoy plane ($-\pi \leq \phi \leq \pi$). It should be noted that for a constant surface of $\xi = (r_1 + r_2)/\alpha$, the scattered energy takes $t = (r_1 + r_2)/c$ seconds to reach to the Rx (where c is the speed of light), and thus we can write $\xi = ct/\alpha$. Suppose that the interval for which it takes for the transmitted unit impulse reflections to reach to the receiver is $t_{min} \leq t \leq t_{max}$ (corresponding to $\xi_{min} \leq \xi \leq \xi_{max}$). Then, as the volume element in the prolate spheroidal coordinates is defined as $\partial V = (\alpha^3/8)(\xi^2 - \eta^2)\partial\xi\partial\eta\partial\phi$, in order to achieve the energy received to the Rx at each t (named $C(t)$), we should consider performing the first two integrations in (10) for η and ϕ as [20]

$$C(t)=\frac{ck_s\exp(-k_e ct)a}{8\pi^2\left(1-\cos\left(\frac{\Theta_T}{2}\right)\right)\alpha^2}\int_{\eta_1(t)\phi_1(t,\eta)}^{\eta_2(t)\phi_2(t,\eta)}\frac{\phi(\Theta_s)\cos\zeta}{(ct/\alpha)^2-\eta^2}d\phi d\eta \tag{11}$$

in which the values for $\eta_1(t)$, $\eta_2(t)$, $\phi_1(t,\eta)$ and $\phi_2(t,\eta)$ are imposed by the geometric model and are obtained by corresponding equations in [20].

Finally to find the total energy (in joules) received at the receiver for the whole delay spread ($t_{min}\le t\le t_{max}$), we should integrate $C(t)$ from t_{min} to t_{max} as in

$$I_{config_B}=\int_{t_{min}}^{t_{max}}C(t)\,dt=(\alpha/c)\int_{\xi_{min}}^{\xi_{max}}C(\xi\alpha/c)\,d\xi. \tag{12}$$

As shown in Fig. 5 B1, the common volume can be divided into two separate regions, resulting in the integral in (12) to be calculated by the summation of two different integrals, one from ξ_{min} to $\xi_{\max_1}$ and the other one from $\xi_{\max 1}$ to $\xi_{\max 2}$. The first integral corresponds to the impulse responses from t_{min} to t'_{max} and the second one corresponds to the impulse responses from t'_{max} to t_{max}. It worth noting that the first part of the integral is considering both sides of the TR line and the second integral is considering the right side of the TR line.

As it is clear from Fig. 5 B1, the first integral starts from the smallest prolate spheroid which is corresponding to the minimum ξ, therefore the lower bound of integral is $\xi_{min_1}=1$. In order to find $\xi_{\max 1}$ and $\xi_{\max 2}$, we have to find the largest prolate spheroids which pass through the intersection of the two cones on the left side and right side of the TR line. To do so, we find the following equations in (13) and (14), inspired by the work in [20].

$$\xi_{\max 1} = m + \sqrt{m^2 - 1} \tag{13}$$

$$\xi_{\max 2} = n + \sqrt{n^2 - 1} \tag{14}$$

where

$$m = \frac{1 + \cos\psi_{R_{max}} \cos\psi_{T\,min}}{\cos\psi_{R_{max}} + \cos\psi_{T\,min}} \tag{15}$$

and

$$n = \frac{1 + \cos\psi_{R_{min}} \cos\psi_{T\,max}}{\cos\psi_{R_{min}} + \cos\psi_{T\,max}} \tag{16}$$

in which $\psi_{R_{min}} = \Theta_R / 2 - \beta_R$, $\psi_{T_{min}} = \Theta_T / 2 - \beta_T$, $\psi_{R_{max}} = \Theta_R / 2 + \beta_R$ and $\psi_{T_{max}} = \Theta_T / 2 + \beta_T$

For the configuration in B2, all the procedure is the same as the one for B1, except the bounds of the integral in (12). This time the common volume is not divided into two parts. Here the lower bound is is clearly different than the previous part and is obtained as ξ_{min2} and is found by (17), while the upper bound is the same as $\xi_{\max_2}$ in B1.

$$\xi_{\min 2} = q + \sqrt{q^2 - 1} \tag{17}$$

where

$$q = \frac{1 + \cos\psi_{R_{min}} \cos\psi'_{T\,min}}{\cos\psi_{R_{min}} + \cos\psi'_{T\,min}} \tag{18}$$

in which $\psi_{T\,min}^{'} = \beta_T - \Theta_T / 2$.

Therefore, the geometric channel for the ground-to-air link in configuration B is

$$I_{config_B} = \begin{cases} \left(\frac{\alpha}{c}\right)\left(\int_{\xi_{\min_1}}^{\xi_{\max_1}} C\left(\xi\alpha / c\right) + \int_{\xi_{\max_1}}^{\xi_{\max_2}} C\left(\xi\alpha / c\right)\right) d\xi \;\; \& \; \xi_{\min_1} = 1, \xi_{\max_1} \; and \; \xi_{\max_2} \; as \; (13) \,\&\, (14) & \text{for config B1} \\ \left(\frac{\alpha}{c}\right)\int_{\xi_{\min_2}}^{\xi_{\max_2}} C\left(\xi\alpha / c\right) d\xi \qquad \& \; \xi_{\min_2} \; as \; (17), \xi_{\max_2} \; as \; (14) & \text{for config B2} \end{cases}$$

(19)

2.2.3 Channel Model for Configuration C

To find the geometric channel for configuration C (shown in Fig. 2), we should notice that the scattering angle in this configuration is more than $\pi / 2$, making us to wonder the feasibility of the phase function in (3) to be used for the backscatter in this case. In order to check this, the plot for the amounts of the generalized scattering model of (3) in Fig. 4 shows that the function is suitable for scattering angles more than $\pi / 2$ and has meaningful amount for configurations like this.

Like configuration B, this configuration also has two possibilities which are shown in Fig. 6 as C1 and C2. All the parameters are the same as configuration B and are shown in the figure.

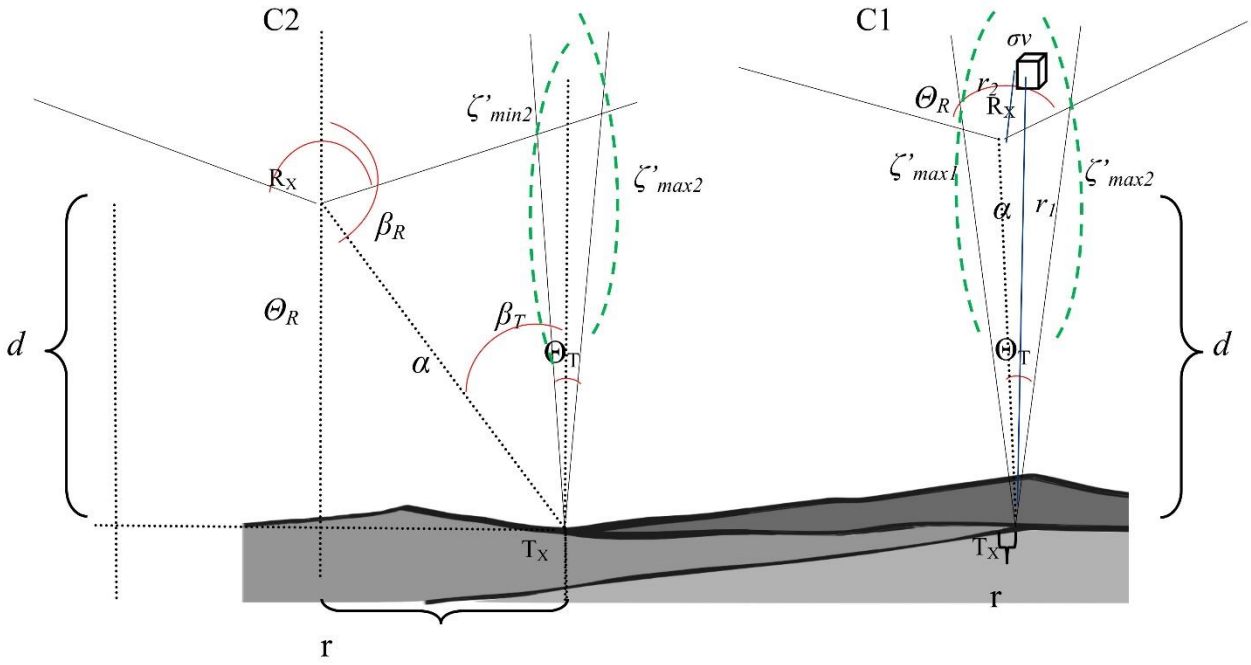

Figure 6: UV link geometrical configuration between ground node (transmitter) and UAV (receiver) in configuration B

Also, the integral bounds in (11) are found according to [20], like the previous configuration. On the other hand, to find the bounds of ξ for the integral in (12), for the configuration in C1, the integral in (12) is divided into two separate integrals, one from ξ'_{min_1} to $\xi'_{\max 1}$ and the other from $\xi'_{\max 1}$ to $\xi'_{\max 2}$. ξ'_{min_1} is clearly the smallest prolate spheroid which is $\xi'_{min_1}=1$ and $\xi'_{\max 1}$ and $\xi'_{\max 2}$ are found by

$$\xi'_{\max 1} = m' + \sqrt{m'^2 - 1} \tag{20}$$

$$\xi'_{\max 2} = n' + \sqrt{n'^2 - 1} \tag{21}$$

where

$$m' = \frac{1+\cos\psi_{R_{min}}\cos\psi_{T\,min}}{\cos\psi_{R_{min}}+\cos\psi_{T\,min}} \tag{22}$$

and

$$n' = \frac{1-\cos\psi_{R_{max}}\cos\psi_{T\,max}}{\cos\psi_{R_{max}}+\cos\psi_{T\,max}} \tag{23}$$

For the configuration in C2, the integral in (12) is not divided into two parts. This time the upper bound of the integral is the same as $\xi'_{\max 2}$ in (21) for configuration C1, while the lower bound of the integral will be ξ'_{min2} as below

$$\xi'_{\min 2} = q' + \sqrt{q'^2 - 1} \tag{24}$$

where

$$q' = \frac{1+\cos\psi_{R_{max}}\cos\psi_{T\,min}^{'}}{\cos\psi_{R_{max}}+\cos\psi_{T\,min}^{'}}\ . \tag{25}$$

As a result, the geometric channel for the ground-to-air link in configuration B is

$$I_{config_C} = \begin{cases} \left(\frac{\alpha}{c}\right)\left(\int_{\xi'_{\min_1}}^{\xi'_{\max 1}} C\left(\xi\alpha/c\right) + \int_{\xi'_{\max 1}}^{\xi'_{\max 2}} C\left(\xi\alpha/c\right)\right) d\xi \ \ \&\ \xi'_{\min_1} = 1, \xi_{\max_1}\ and\ \xi_{\max_2}\ as\ (20)\ \&\ (21) & \text{for config C1} \\ \left(\frac{\alpha}{c}\right)\int_{\xi'_{\min_2}}^{\xi_{\max 2}} C\left(\xi\alpha/c\right) d\xi \qquad \&\ \xi'_{\min_2}\ as\ (24), \xi_{\max_2}\ as\ (21) & \text{for config C2} \end{cases}$$

(26)

CHAPTER III

ULTRAVIOLET COMMUNICATIONS FOR GROUND-TO-AIR LINKS

3.1 Introduction

The current research on ultraviolet communications has not paid enough attention to the high capabilities of this medium for UAV communications. To the best of our knowledge, UV communications in the context of UAV links has been investigated in a recent work which focuses on UAV networks [39]. This paper discusses the connectivity issues in a mobile UAV UV-based communications network. As in that work the writers are investigating the connectivity issues, and also as the nature of UV geometric channel model is complicated, they have chosen to work with the simplest channel model possible, which is the one introduced in [27]. The problem with using that model is that it is based on two parameters (path loss factor and path loss exponent) which are not defined based on the geometry of the UV link configuration and are measured by some experiments for some limited specific configurations for which the experiment has been performed. In other words, those two parameters are not mathematically functions of the geometric configuration of the channel. This issue causes this model not to be adequate to show the variations caused by the changes in the geometric parameters during the movement. Therefore, in order to be able to use this model, in [39], the writers have assumed all the nodes in the network to have the same altitude of flight. Therefore, the changes in the channel geometric path loss during the movement have not been depicted in that work.

In this work, in order to completely include the geometric variations in our study, we first introduced the channel for ground-to-UAV UV communication in chapter II and we will use those models in different configurations in this chapter.

In this chapter, we consider the uplink of an unattended ground sensor [14], where a number of sensor nodes are placed on the ground in a serial manner and with equal intra-distances. A UAV periodically visits the area and collects the sensor data from ground nodes. For the uplink transmission under consideration, we investigate the performance of UV-based aerial system and determine the maximum UAV coverage to maintain a pre-defined bit error rate (BER) performance.

3.2 System Model

As illustrated in Fig. 7, we consider the uplink of a network with N sensor nodes placed on the ground in a serial manner and with equal intra-distances. The UV transmitters in ground sensors face upwards. In order to study the effects of different configurations on the performance and to compare the performance of different configurations together and be able to choose the best one based on one's need, three different scenarios are considered in which, the UV receiver on the aerial vehicle is located in three different configurations. As shown in Fig.7, the configurations are named A, B and C in correspondence to the channel models introduced in the previous chapter.

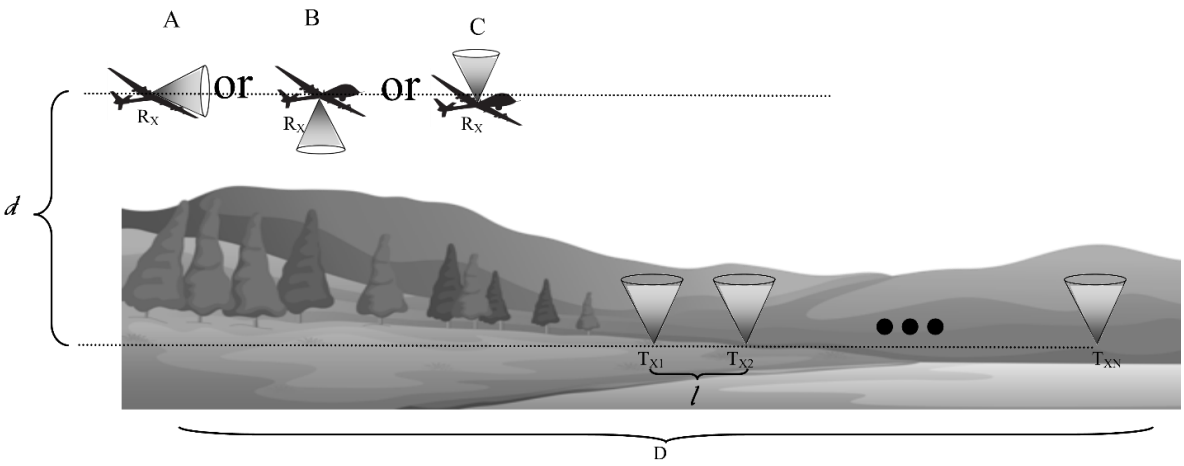

Figure 7: Sensor network under consideration

The end-to-end distance is D and therefore the intra-distance between consecutive ground nodes is equal to $l = D / N$. The receiver is placed at the UAV which flies at a height of d meters above the ground. It communicates with each ground node on a one-by-one basis. Therefore, without loss of generality, we consider only the communication with a specific node as illustrated in Figures 3,5 and 6 in chapter 2 (depending on the configuration of the UAV receiver). All the parameters are the same as the previous chapter. Here, we assume that the transmitter beam divergence is smaller than the receiver field of view (which is logical due to the UV LEDs and detectors which exist in the industry [11]). Therefore, depending on the configuration of the receiver, the optical received power (irradiance) which is received can be calculated by (7) for configuration A, (19) for configuration B or (26) for configuration C.

We consider a system with intensity modulation and direct detection (IM/DD). Let $s \in \{0,1\}$ denote the on-off keying (OOK) modulation symbol transmitted from the sensor node. The received signal is given by

$$y = \eta I(r)s + w \quad (27)$$

where η is the optical-to-electrical conversion coefficient and $I(r)$ was already defined in previous chapter (depending on the configuration, whether (), () or ()) in terms of system parameters. In (27), w is the additive white Gaussian (AWGN) noise term with zero mean and variance of $\sigma_w^2 = N_0/2 = 2hfR$, where h is the Planck constant, f is the carrier frequency and R is the system bandwidth [42].

3.3 Maximum UAV Coverage for a Targeted BER

In this section, we determine the maximum coverage of UAV, i.e., maximum value of horizontal distance denoted by r_{max}, while satisfying a predefined BER target. The minimum number of the required transmitters to cover a distance of D can be then obtained as $N_{min} = D / r_{max}$.

In order to do so, we have to consider the differences between the configurations shown in Fig. 7, as the optical power which is received in the detector is different in each of them.

3.3.1 Maximum UAV Coverage for Configuration A

For this configuration, the optical power which is received by the detector is obtained by (7). Using Taylor series[1], we can approximate the exponential term in (7) as $\exp(k_e r) \approx 1 + k_e r$. Replacing r by r_{max} therein, we have the minimum required irradiance as

[1] For clear weather conditions in UV-C frequencies, k_e is in the order of 10^{-3}. Considering that the horizontal distance r is a few hundreds of meters in our case, $k_e r_{max}$ is in the order of 10^{-1}.

$$I_{\min} \simeq A\left(\frac{1}{r_{\max}} + Br_{\max}\right)\frac{1}{1+k_e r_{\max}} \tag{28}$$

which can be written in a quadratic form of $\left(I_{min}k_e - AB\right)r_{max}^2 + I_{min}r_{max} - A = 0$. Solving this equation for $r_{max} > 0$ we have

$$r_{\max} = \frac{\sqrt{I_{\min}^2 + 4A(I_{\min}k_e - AB)} - I_{\min}}{2\left(I_{\min}k_e - AB\right)} . \tag{29}$$

Let BER_{max} denote the targeted BER. The BER of OOK modulation [42, 43] is given by

$$BER = Q\left(\frac{1}{2}\sqrt{\frac{\eta I(r)}{2hfR}}\right) \tag{30}$$

where $Q(.)$ denotes the Gaussian Q-function. The minimum irradiance I_{min} to achieve this is then calculated as

$$I_{\min} = \frac{8hfR\left(Q^{-1}\left(BER_{\max}\right)\right)^2}{\eta} \tag{31}$$

where $Q^{-1}(.)$ is the inverse Gaussian Q-function. Replacing (9) in (7), we can find the maximum horizontal distance to satisfy the BER_{max}.

3.3.2 Maximum UAV Coverage for Configurations B and C

For the two configurations of B and C, the received optical irradiance in the receiver is given by (19) and (26) respectively. For these two configurations, there is no closed form for the optical irradiance, as it was discussed in the previous chapter. Therefore, to find the maximum UAV coverage (i.e. r_{max}), we have to find the irradiance for different horizontal distances between the transmitter and the receiver numerically and then find the maximum

coverage for that configuration, by intersecting the irradiance curve vs different distances with the minimum required irradiance I_{min} for a targeted BER_{max} from (31).

There is also one other difference between the configurations here. As it was mentioned before, for an ultraviolet communication link to be established, there should be a common volume between the transmitter and receiver cones of the link. As it is seen from Fig. 3, for case A, the communication link is established between the transmitter and the receiver, while the receiver is approaching the transmitter, but not when the receiver has passed above the transmitter node. On the other hand, for case B, even when it is approaching the transmitter node, there is no guarantee that a link exists, and that is because there is not always a common volume between the transmitter and receiver cones. In order to find the horizontal distance, for which there exists a common volume between the transmitter and the receiver, the critical condition in which the communication link is going to be formed between the cones, is shown in Fig. 8. We call this horizontal distance as r_{critic}. As we have assumed that $\Theta_R > \Theta_T$, it is clear from the figure that as the UAV-based receiver is approaching the ground-based transmitter, the first time for which a common volume exists between the transmitter and receiver cones, is when $r_{critic} = d \times \tan^{-1}(\Theta_R/2)$. It is also clear from the symmetry of the trajectory of the receiver in configuration B that when it passes the transmitter, still there is communication link between the transmitter and the receiver, until it passes r_{critic} meters after the transmitter. The link stops working, when the received optical irradiance drops below the required amount of I_{min}, and then the communication link is established between the UAV and the new transmitter which UAV is approaching to.

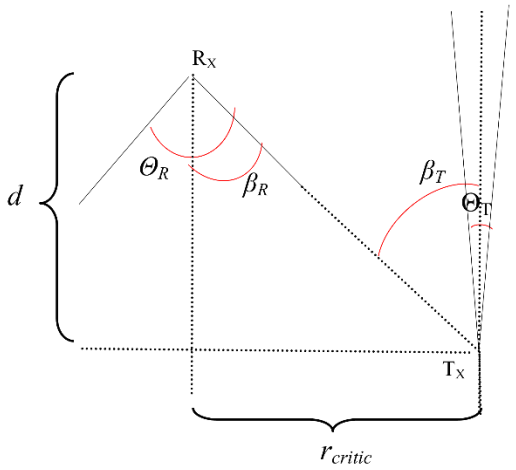

Figure 8: Critical condition for configuration B

Also, for configuration C, we have to notice that not only there is always a communication link between the transmitter and the receiver as the transmitter is approaching the receiver, but also the communication link exists even after that the receiver has passed above the transmitter.

3.4 Minimum Number of Required Sensors

The maximum UAV coverage for a targeted BER_{max} determines the distance within which the BER is less than or equal the targeted value during the time when drone is approaching the transmitter and therefore, before or after this coverage area, there should be another ground-based transmitter to maintain the BER. Therefore, as the UAV-based receiver passes the coverage distance of a single one-by-one link, the contact with the next transmitter begins. Thus, the minimum number of ground-based transmitter sensor nodes to cover a total distance of D is $N_{min} = D / r_{max}$.

3.5 Numerical Results and Discussion

In this section, we present numerical results for the UV systems under consideration. System and channel parameters are provided in Table I and used in the following figures unless otherwise noted. All the parameters are the same for all the three configurations of A,B and C, in order to be fair and make comparison possible.

Table I System and channel parameters units

Transmitter beam divergence (Θ_T)	5^o
Receiver field of view (Θ_R)	30^o
End-to-end distance (D)	1000 m
Targeted BER ($BER_{\max}$)	10^{-6}
Atmospheric absorption coefficient (k_a)	$0.74\,\text{km}^{-1}$
Rayleigh scattering coefficient (k_s^{Ray})	$0.24\,\text{km}^{-1}$
Mie Scattering coefficient (k_s^{Mie})	$0.25\,\text{km}^{-1}$
Optical-to-electrical conversion coefficient (η)	2%
Wavelength (λ)	254 nm
Receiver aperture Are (a)	$7.07\ \text{cm}^2$
System bandwidth (R)	5 kbps
Planck's constant (h)	$6.62\times10^{-34}\ \text{m}^2\text{kg.s}^{-1}$

In Fig. 9, we illustrate the received irradiance based on (7) for a UAV flying towards the ground-based transmitter assuming different flight heights (d) for the configuration A. The UAV is initially 200 m away ($r = 200$ m) and moves towards the transmitter. It is seen that the received power increases in an exponential manner since the first term of (2) dominates. To achieve the targeted $BER_{max} = 10^{-6}$, we calculate the minimum required irradiance from (9) as indicated by a constant line in Fig.9. The intersection points with the

plots associated with different d values are further indicated by "*". For example, assume d=200 m. Our results show that to satisfy the targeted BER value, the maximum UAV coverage (r_{max}) is equal to 109.14 m. This decreases to 87.35, 69.61, 55.78 and 44.42 m for d=400, 600, 800 and 1000 m, respectively.

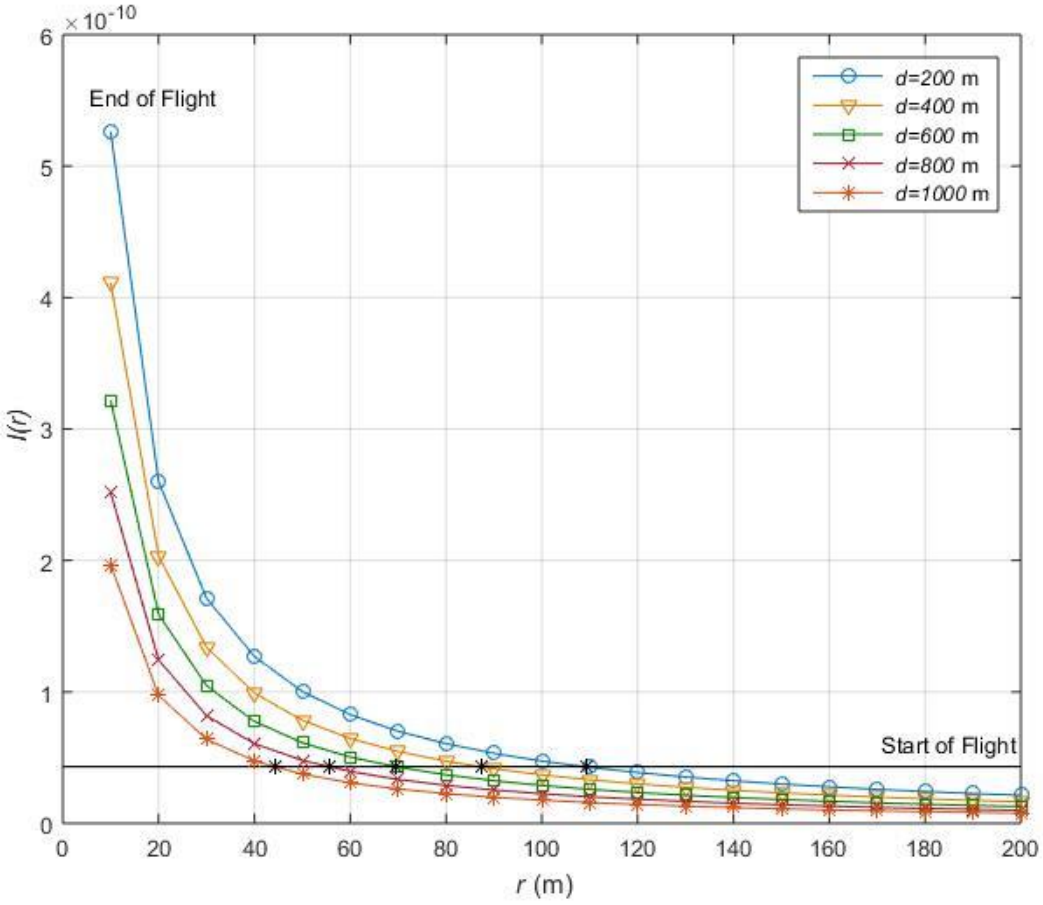

Figure 9: Received irradiance with respect to distance for different flight heights for configuration A

In Fig. 10, we illustrate the received irradiance for configuration A based on (7) for a UAV flying at a height of d = 400 m considering different values of BER_{max}. It is observed that when BER_{max} is lower (i.e. better performance), the required minimum irradiance will be higher. This decreases the maximum UAV coverage. Specifically, it is observed that for

$BER_{max} = 10^{-3}$, we have r_{max} = 183.85 m. This decreases to 134.65, 106.04, 87.35 and 74.30 m for $BER_{max} = 10^{-4}, 10^{-5}, 10^{-6}$ and 10^{-7} respectively.

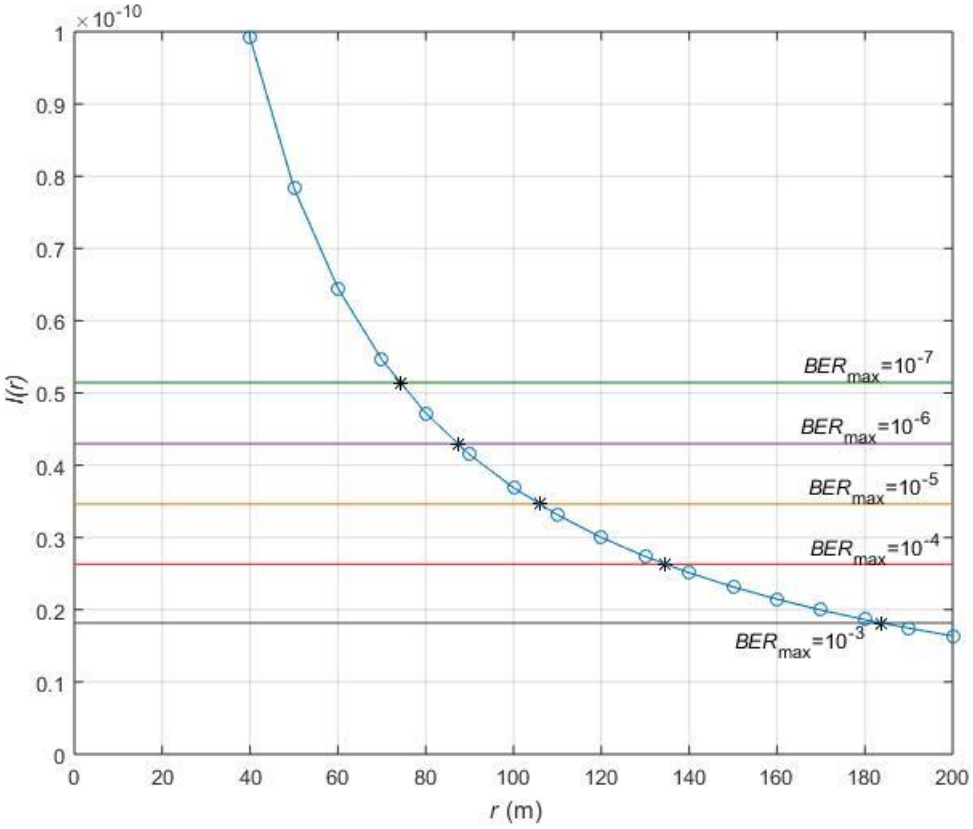

Figure 10: The effect of required BER_{max} on UAV coverage for configuration A

In order to illustrate the change of irradiance for different flight heights for configuration B, we first have to calculate r_{critic} for each flight height. Amounts of r_{critic} for five different heights are written in table II.

Table II r_{critic} for different flight heights for configuration B

Flight Height (d)	200 m	400 m	600 m	800 m	1000 m
r_{critic}	51.21 m	102.42 m	153.63 m	204.84 m	256.05 m

As it was expected, the value of r_{critic} increases as the flight height increases, i.e. if the drone is flying in a higher distance, as the receiver is flying towards the transmitter, the connection between the transmitter and the receiver is stablished sooner.

As all the values in the table are less than 51.21 m, we illustrate the received irradiance for configuration B in Fig. 11, based on (16), for horizontal distance of less than 51.21 m, i.e. the UAV is initially 51.21 m away ($r = 51.21$ m) and moves towards the transmitter. The same maximum required error rate of $BER_{max} = 10^{-6}$ is targeted, meaning the same minimum required irradiance from (31) is indicated by a constant line in Fig. 10. We illustrate the received irradiance based on (16) for a UAV flying towards the ground-based transmitter assuming different flight heights (d) for the configuration B. The intersection is indicated by "*". According to the symmetry which was discussed in the section 3.3.2, the maximum UAV coverage for this configuration is double the amount of intersections. Therefore, to satisfy the targeted BER value, the maximum UAV coverage (r_{max}) for configuration B is equal to 54.84 m, 64.15 m, 59.34 m, 49.80 m and 40.06 m for d =200, 400, 600, 800 and 1000 m, respectively. As it is seen, in this configuration as the flight height increases, the maximum coverage first increases and then decreases. The reason is that, as the height increases, the common volume between the transmitter and receiver cone enlarges, while the bird-fly distance of the transmitter and the receiver (α in Fig. 5) is also increasing. Until a certain height, the positive effect of increase of the common volume is more than the negative effect of increase of the bird-fly distance, thus the maximum coverage increases, while after that certain height, the bird0fly distance is long enough to dominate the common volume and cause the maximum coverage to drop.

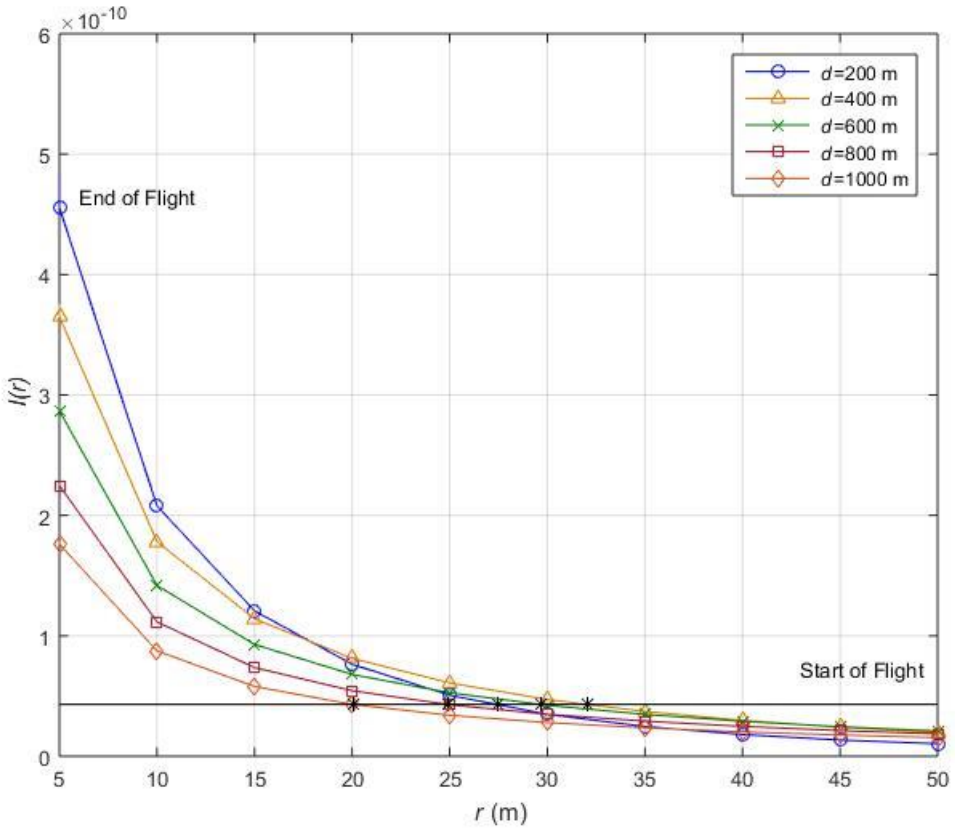

Figure 11: Received irradiance with respect to distance for different flight heights for configuration B

In Fig. 12, we present the maximum UAV coverage (r_{max}) for configuration A based on (29) assuming different values of transmitter beam divergence (Θ_T) and receiver FOV (Θ_R) assuming a flight height of d = 100 m. It is observed that r_{max} takes small values if Θ_R is small. With increase in Θ_R, r_{max} increases. It is further observed that the value of r_{max} is almost independent of Θ_T within the range of values under consideration.

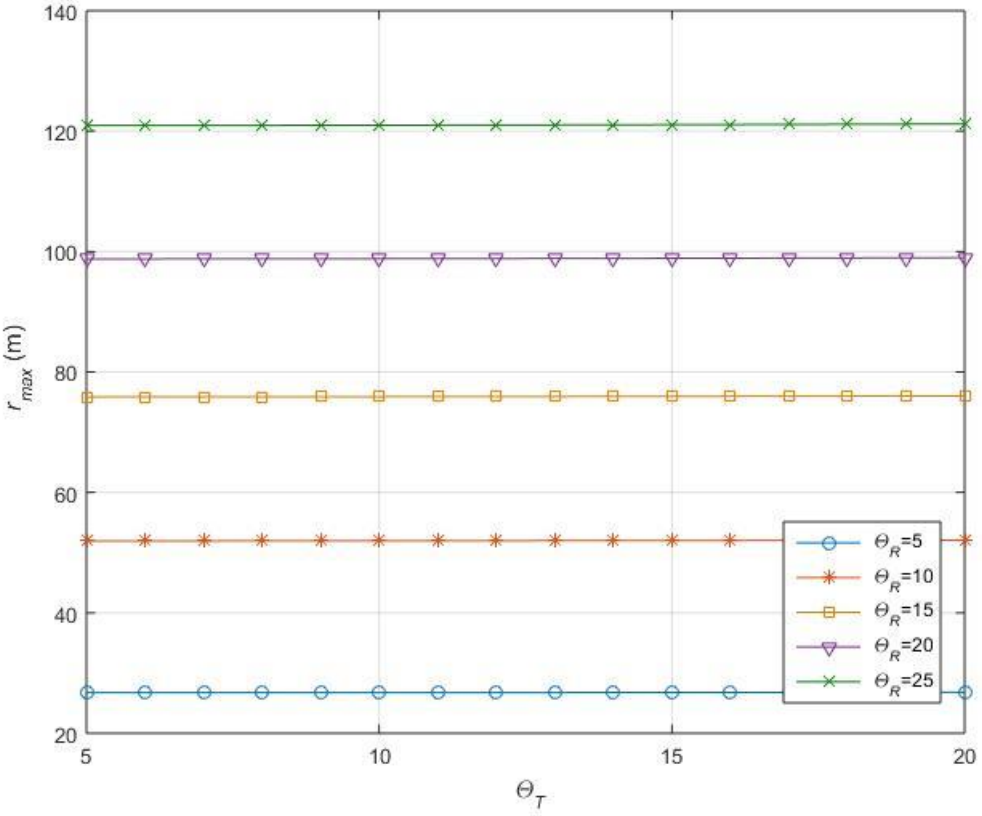

Figure 12: The effect of receiver FOV and transmitter beam divergence on UAV coverage for configuration A

In Fig. 13, we present the maximum UAV coverage (r_{max}) and the minimum number of required sensors (N) with respect to receiver FOV (Θ_R) assuming different values of flying heights (d) for configuration A. We assume a fixed transmitter beam divergence of $\Theta_T = 5$. It is observed that the more the flight height of the UAV, the less the maximum coverable horizontal distance. The minimum number of required transmitters (N) to cover the total distance of $D = 1000$ m obviously decreases when r_{max} increases.

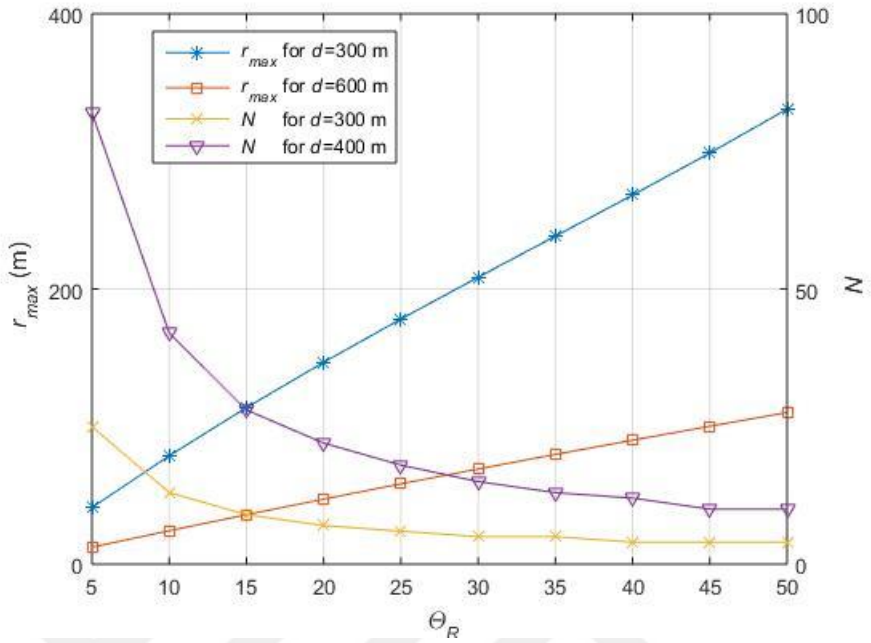

Figure 13: The effect of flying height on UAV coverage for Configuration A

CHAPTER IV

ULTRAVIOLET COMMUNICATIONS FOR GROUND-TO-AIR LINKS IN PRESENCE OF INTERFERANT CHANNELS

4.1 Introduction

In the previous chapter, we studied the uplink of a ground sensor network, in which the ground-based transmitters were communicating with the UAV-based receiver in a one-by-one basis. Therefore, in that system, there is no interference involved and the other transmitters in the sensor network do not interfere with desired ultraviolet communication link which is established while the receiver is approaching the transmitters (as in case A) or approaching and departing from the transmitters (as in case B and C). In this chapter, we aim to study the effect of the interference of the other ground-based transmitters on the performance of the links. Therefore, we will study the system in which the communication link between the transmitter and the receiver is not one-by-one and other transmitters are interfering with the main UV link. Also, we tend to investigate the effect of deterministic and random placement on the system performance. Therefore, in this chapter, we first consider a system in which the ground-based transmitter nodes are placed with equal intra-distances and then study a system in which the transmitter nodes are placed randomly.

4.2 System with Equidistantly-Placed Ground-Based Transmitters

4.2.1 System Model

As it was illustrated in Fig.7, we consider the uplink of a network with N sensor nodes placed on the ground in a serial manner and with equal intra-distances of l. The UV

transmitters in ground sensors face upwards. The receiver is placed on the UAV such that the receiver cone is facing the horizontal axis, and is approaching the first transmitter on its right side. The UAV is flying at a height of d meters above the surface. The communication link is intended to be established with the nearest ground-based transmitter, but as the other transmitters may also transmit signals, there might be interference involved in the communication. Once the receiver passes from one of the transmitters, the next node becomes the main transmitter and the others on its right remain as the interferes for the new link. Therefore, each time the nodes on the left side of the receiver have no effect on the link (as they are not seen by the receiver), the nearest node on the right of the receiver is the main transmitter and the other nodes on the right of the main transmitter play the role of interferers.

Assume that in addition to the intended transmitter, there are k more transmitters on the right side of the receiver. The horizontal distance between the transmitter and the main receiver is denoted by r_0, while the horizontal distance between the interferent transmitters and the receiver is shown by r_1, r_2,…, r_k. The receiver field of view is Θ_R. In order to keep all the configurations between the transmitters as identical as possible, all the transmitters have the same beam divergence denoted by Θ_T. The UV channel between each transmitter (whether the main transmitter or one of the interferents) is like the one shown in Fig. 3 in chapter 2. Therefore the UV channel for each communication link can be obtained form (7). As it was proved in chapter 2 that the UV channel in this configuration is a function of the horizontal distance between the transmitter and the receiver, the channel for the main communication link between the main ground-based transmitter and the UAV-based receiver is written as a function of its horizontal distance to the receiver as $I(r_0)$, while the channel

between the interferent receivers and the transmitter is written as a function of each of their distances to the receiver as $I(r_1),\ I(r_2),\ \ldots,\ I(r_k)$.

We consider a system with intensity modulation and direct detection (IM/DD). If $s_i \in \{0,1\},\ i \in \{0,1,\ldots,k\}$ denotes the on-off keying (OOK) modulation symbol which is transmitted from the i th transmitter and all the ground-based sensor nodes transmit the same power of Q_T, then the received signal in the receiver is given by

$$y = \eta Q_T I(r_0) s_0 + w + \eta \sum_{i=1}^{k} Q_T I(r_i) s_i u_i \tag{32}$$

where η is the optical-to-electrical conversion coefficient and w is the additive white Gaussian (AWGN) noise term with zero mean and variance of $\sigma_w^2 = N_0 / 2 = 2hfR$, where h the Planck constant, f is the carrier frequency and R is the system bandwidth. u_i is an indicator which shows if the i th sensor node transmits with how much probability. u_i is 1, when the i th transmitter is transmitting with the probability of p and is 0 when the i th transmitter does not have any signal to send, with probability of $1-p$. It is assumed that we are investigating the performance of the intended transmitter for the non-idle time and therefore there is no such an indicator like u_0. used for the first term in (32).

4.2.2 Interference and Noise Characterization

In this part, we aim to characterize the interference in (32) as a random variable and then characterize the summation of noise and interference as another random variable. We define random variable v as the summation of the noise and the interference in (32). We

call the resulted interference from each of the interferer nodes as z_i and we call the whole interference as Z, i.e.

$$v = w + Z, \quad Z = \sum_{i=1}^{k} z_i, \quad z_i = \eta Q_T I\left(r_i\right) s_i u_i \tag{33}$$

As it was mentioned $s_i \in \{0,1\}$ is the on-off keying symbol which is transmitted by the i th sensor. As the receiver does not have knowledge of the transmitted symbol from each of the sensor nodes, s_i can be assumed as a random variable in receiver's point of view. If we assume that when the transmitter has a signal to send, the probability of transmission of 0 and, the probability of sending 1 are the same, then the following probability density function (PDF) can be written for the s_i :

$$f_{s_i}(s) = \begin{cases} \frac{1}{2} & is\ s = 0 \\ \frac{1}{2} & is\ s = 1 \end{cases} \tag{34}$$

The PDF in (4-3) can also be written $f_{s_i}(s) = (1/2)\delta(s-1) + (1/2)\delta(s)$, where $\delta(.)$ is the Dirac delta function.

For the parameter u_i in (33), the following pdf can be written with the same procedure:

$$f_{u_i}(u) = \begin{cases} p & is\ u = 1 \\ 1-p & is\ u = 0 \end{cases} \tag{35}$$

which can be rewritten as $f_{u_i}(u) = p\delta(u-1) + (1-p)\delta(u)$.

Multiplication of s_i and u_i forms a new random variable which we denote it as γ_i and has the following PDF:

$$f_{\gamma_i}(\gamma)=\left(\frac{1}{2}\right)p\delta(\gamma-1)+(1-p)\delta(\gamma) \tag{36}$$

The reason is that the i th transmitter whether has a signal to send (either 0 or 1, each with probability of 0.5) or it is idle.

By using (7) from chapter 2, the conditional mean for each random variable of z_i is

$$E(z_i|\gamma_i)=\eta Q_T I(r_i)\gamma_i=\eta Q_T A\exp(-k_e r_i)\left(\frac{1}{r_i}+Br_i\right)\gamma_i \tag{37}$$

Therefore, the mean and variance of the random variable z_i is

$$E(z_i)=\eta Q_T A\exp(-k_e r_i)\left(\frac{1}{r_i}+Br_i\right)\int_{-\infty}^{\infty}E(z_i|\gamma_i)\,f_{\gamma i}(\gamma)\,d\gamma \tag{38}$$

By substituting (4-6) in (4-7) and after some mathematical manipulation, the mean of random variable z_i is

$$\mu_{z_i}=\frac{p}{2}\eta Q_T A\exp(-k_e r_i)\left(\frac{1}{r_i}+Br_i\right) \tag{39}$$

As variance of z_i is $\sigma_{z_i}^2=E\left(z_i^2\right)-\left(E(z_i)\right)^2$, in order to find it, we first have to find $E\left(z_i^2\right)$. Through the same procedure of (4-7) and (4-8), first we have

$$E\left(z_i^2|\gamma_i\right)=\eta^2 Q_T^2\left(I\left(r_i\right)\right)^2\gamma_i^2=\eta^2 Q_T^2 A^2\exp\left(-2k_e r_i\right)\left(\frac{1}{r_i}+Br_i\right)^2\gamma_i^2 \tag{40}$$

Therefore,

$$\sigma_{z_i}^2=\frac{p}{2}\eta^2 Q_T^2 A^2\exp\left(-2k_e r_i\right)\left(\frac{1}{r_i}+Br_i\right)^2 \tag{41}$$

The random variables of z_i satisfy the conditions of the Lyapunov central limit theorem [44], therefore for sufficiently large number of interferers (i.e. large k), we can approximate the sum of random variables z_i (named Z) as a gaussian random variable with mean and variance of $\mu_Z=\sum_{i=1}^{k}\mu_{z_i}$ and $\sigma_Z^2=\sum_{i=1}^{k}\sigma_{z_i}^2$.

The sum of two gaussian random variables is another gaussian with mean and variance of the total mean and variance of each of them respectively. As a result, we can find the PDF of the summation of the noise and interference (i.e. random variable v in (32)) as another gaussian random variable with mean and variance of $\mu_v=\mu_Z$ and $\sigma_v^2=N_0/2+\sigma_Z^2$.

4.2.3 Bit Error Rate Performance

Now that we have found the PDF of the sum of added terms to the intended received signal in (4-1), we can find the bit error rate performance based on that. We consider that the receiver which works based on maximizing a posteriori probability. The maximum a posteriori or MAP criterion turns into maximum likelihood, if the probabilities of sending

different symbols of a modulation are the same, which it is in our case. Thus, the error probability for our system will be $p_e = Q\left(\frac{1}{2}\sqrt{\frac{\eta Q_T I(r_0)}{\sigma_\nu}}\right)$ [42].

Inserting the values of μ_ν, σ_ν and $I(r_0)$ into P_e, we will have the error rate performance for the UV communication for air-to-ground links in presence of other UV links interference as

$$BER = Q\left(\frac{1}{2}\sqrt{\frac{\eta Q_T A exp(-k_e r_0)\left(\frac{1}{r_0}+Br_0\right)}{(p/2)\eta^2 {Q_T}^2 \sum_{i=1}^{k}\exp(-2k_e r_i)\left(\frac{1}{r_i}+Br_i\right)^2 + 4h^2 f^2 R^2}}\right) \quad (42)$$

And as the distance between the ground-based nodes is the same, therefore $r_i = r + il$ ($i \in \{1, 2, \ldots, k\}$). Substituting r_i in (42), we have

$$BER = Q\left(\frac{1}{2}\sqrt{\frac{\eta \exp(-k_e r_0) A\left(\frac{1}{r_0}+Br_0\right)}{(p/2)\eta^2 {Q_T}^2 \exp(-2k_e r_0)\sum_{i=1}^{k}\left(\exp(-k_e il) A\left(\frac{1}{r_0+il}+B(r_0+il)\right)\right)^2 + 4h^2 f^2 R^2}}\right) \quad (43)$$

4.3 System with Randomly-Placed Ground-Based Transmitters

4.3.1 System Model

The system model in this scenario is the same as the previous case, except that the intra-distances between the interferers (i.e. the ground-based transmitters on the right side of the UAV-based receiver) are not the same and the receivers are distributed randomly. Except that, All the system parameters and channel model parameters are the same as previous case in section 4.2.

Here, the nodes are distributed randomly on the horizontal surface, in a serial manner. In order to include a general case of random placement, we consider the homogeneous Poisson point process (abbreviated as PPP). We denote the point process parameter as Λ. This parameter is the node linear density, i.e. the mean value of the number of nodes placed on a unit line. We also assume Λ to be constant, as we want to consider a uniform node placement scenario. With that in mind, the probability that n nodes are placed on a hypothetical line of ST with length of L is

$$Prob\{n\ nodes\ on\ ST\} = \frac{\exp(-\Lambda L)(\Lambda L)^n}{n!} \tag{44}$$

In addition to that, as the transmitter nodes are distributed in a random manner, we should provide the probability distribution function of the horizontal distance between the interferent nodes and the receiver. As it was said above, the nodes are uniformly distributed, thus the PDF of the horizontal distance of each node is $f_{r_i}(r) = 1/D$, in which D is the total distance for which the ground sensor network is going to cover.

The received signal in this scenario is the same as the previous one in (4-1).

4.3.2 Interference and Noise Characterization

For this section, all the variables in the previous section are defined the same in this section. In order to characterize the interference in (4-2), this time we first have to find the conditional mean of the random variable of z_i with respect to γ_i. As both r_i and γ_i are random, the conditional mean is

$$E\left(z_i|\gamma_i,r_i\right)=\eta Q_T I\left(r_i\right)\gamma_i=\eta Q_T A\exp\left(-k_e r_i\right)\left(\frac{1}{r_i}+Br_i\right)\gamma_i \tag{45}$$

Therefore, the conditional mean with respect to only γ_i is

$$E\left(z_i|\gamma_i\right)=\int_{R_g}^{D}E\left(z_i|\gamma_i,r_i\right)f_{r_i}\left(r\right)dr_i \tag{46}$$

in which R_g is a guard distant, meaning the minimum distant that two nodes are not going to be assumed to be placed in the same spot as one single transmitter. Inserting $f_{r_i}\left(r\right)=1/D$ and (45) into (46) and using the fact that exponential integral is defined as $E_1\left(x\right)=\int_x^\infty \exp\left(-t\right)/tdt$, after some mathematical manipulation, we have

$$E\left(z_i|\gamma_i\right)=\frac{A\gamma_i Q_T}{\boldsymbol{D}}\left(E_1\left(k_e R_g\right)-E_1\left(k_e D\right)-\frac{B}{k_e}\left(\left(D+\frac{1}{k_e}\right)\exp\left(-k_e D\right)-\left(R_g+\frac{1}{k_e}\right)\exp\left(-k_e R_g\right)\right)\right) \tag{47}$$

Therefore, the mean of the random variable z_i is

$$\mu_{z_i}=\frac{p}{2}\frac{A\gamma_i Q_T}{D}\left(E_1\left(k_e R_g\right)-E_1\left(k_e D\right)-\frac{B}{k_e}\left(\left(D+\frac{1}{k_e}\right)\exp\left(-k_e D\right)-\left(R_g+\frac{1}{k_e}\right)\exp\left(-k_e R_g\right)\right)\right) \tag{48}$$

To calculate the variance of z_i, we first need to have $E(z_i^2)$. Thus, we first obtain $E(z_i^2|\gamma_i)$ with the same steps and some mathematical manipulation:

$$E(z_i^2|\gamma_i) = \frac{(A\gamma_i Q_T)^2}{D-R_g}\left(2k_e\left(E_1(k_eD)\right) - E_1\left(2k_eR_g\right) - \left(B^2\left(\frac{2k_ex_i(k_ex_i+1)+1}{4k_e^3}\right)\exp(-2k_ex_i)\right)\right]_{x_i=R_g}^{x_i=D} + (2B\,\frac{\exp(-2k_ex_i)}{2k_e})_{x_i=R_g}^{x_i=D}\Bigg) \quad (49)$$

Thus $E\left(z_i^2\right)=\left(p/2\right)E\left(z_i^2|\gamma_i\right)$ and therefore the variance of z_i is found through $\sigma_{z_i}^2 = E\left(z_i^2\right)-\left(E\left(z_i\right)\right)^2$.

As the set of the random variables of z_i satisfy the Lyapunov central limit theorem, we approximate the sum of them as a gaussian with mean and variance of the summation of their mean and variance. Therefore, the summation of the noise and interference is a gaussian random variable with the mean and variance of $\mu_\nu = \mu_Z$ and $\sigma_\nu^2 = N_0/2+\sigma_Z^2$ respectively.

4.3.3 Bit Error Rate Performance

To find the bit error rate performance in this scenario, we should notice that the number of interferers is random and the probability of having a certain number of nodes in a certain length is given in (44). Having this in mind and considering (42), we have

$$BER = \sum_{i=1}^{k} Q\left(\frac{1}{2}\sqrt{\frac{\eta I(r_0)}{\sigma_\nu}}\right)\frac{\exp\left(-\Lambda L\right)\left(\Lambda L\right)^i}{i!} \quad (50)$$

4.4 Numerical Results and Discussion

In this section, we present numerical results for the two system models discussed in the previous sections. System and channel parameters are the same as Table I in chapter 3, unless otherwise noted. The flight height is 400 m.

Fig. 13 shows the effect of intra-distance of l on the performance of the main link. To plot this figure, the number of interferers is assumed to be 10. As it is shown, when the

intra-distance of the interferent nodes increases, the BER decreases. That is because by increase in the intra-distance, the interferent nodes are placed in a farer position, resulting in their effect to deteriorate. To plot this figure, the number of interferers is assumed to be 10.

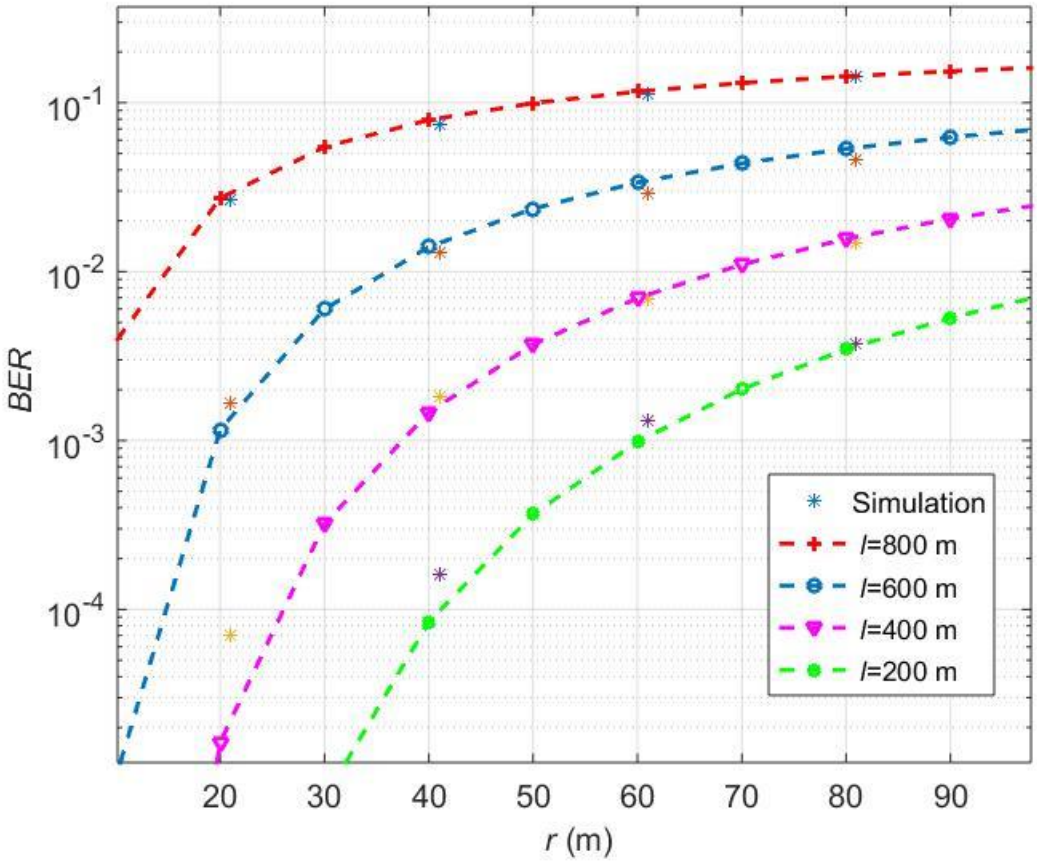

Figure. 14: The effect of intra-distances between the interferent nodes on the performance

CHAPTER V

CONCLUSIONS

In this thesis, we investigate using ultraviolet communications for airborne links. Specifically we considered the use of VU communication for ground-to-air links for an unattended ground sensor network.

Firstly, we mentioned the difference of using UV communications for airborne links than the normal; applications of UV communications and demonstrated that for using UV communications for airborne links, we need to introduce new forms for the NLOS channel modeling. We then introduced the corresponding channel models for different configurations in ground-to-air UV communication.

Later, in the next part, we investigated the concept of UV communication for one-by-one communication links in the uplink of a ground sensor network, discussed the performance and found the maximum coverage for each link in order to maintain a minimum predefined bit error rate.

Finally, in the fourth part, we investigated UV communication links in ground-to-air communications, in presence of interference from other ground-to-air links present in the network. We analyzed the system performance under the assumptions of equidistantly-placed sensors and randomly-placed sensors.

BIBLIOGRAPHY

[1] Uysal, M., & Nouri, H. (2014). Optical wireless communications, An emerging technology, in 2014 16th International Conference on Transparent Optical Networks (ICTON). IEEE

[2] S. Arnon, J.R. Barry, G.K. Karagiannidis, R. Schober, and M. Uysal (Eds.): Advanced Optical Wireless Communication, Cambridge University Press, July 2012

[3] G. Shaw, A.M.Siegel, and M.L.Nischan, \Demonstration system and applications for compact wireless ultraviolet communications," in AeroSense 2003, pp. 241-252, International Society for Optics and Photonics, 2003

[4] M. Uysal, C. Capsoni, Z. Ghassemlooy, A. Boucouvalas, and E. Udvary, Eds., Optical Wireless Communications- An Emerging Technology. Springer International Publishing, 2016.

[5] G. L. Harvey, “A survey of ultraviolet communication systems,” Naval Research Laboratory Technical Report , Washington D.C., March 13, 1964.

[6] Zhengyuan Xu, & Sadler, B. M. (2008). Ultraviolet Communications: Potential and State-Of-The-Art. IEEE Communications Magazine, 46(5), 67–73.

[7] D. M. Reilly, “Atmospheric optical communications in the middle ultraviolet,” *M.S. Thesis*, MIT, Cambridge, MA, 1976

[8] E. S. Fishburne, M. E. Neer, and G. Sandri, “Voicecommunication via scattered ultraviolet radiation,” finalreport of Aeronautical Research Associates of Princeton,Inc., NJ, February 1976.

[9] J. J. Puschell and R. Bayse, “High data rate ultraviolet communication systems for the tactical battlefield,” Proc. IEEE Tactical Commun. Conf. (IEEE, 1990), pp. 1253–267.

[10] Tesar, J. C., & Tesar, C. B. (1994). Optical endoscopic instrumentation in otolaryngology: manufacturer’s and clinician’s points of view. In R. R. Anderson (Ed.), Laser Surgery: Advanced Characterization, Therapeutics, and Systems IV.

[11] Zhengyuan Xu, & Sadler, B. M. (2008). Ultraviolet Communications: Potential and State-Of-The-Art. IEEE Communications Magazine, 46(5), 67–73.

[12] Silicon Carbide UV Avalanche Photodiode (APD), Retrieved from http://www.eoc-inc.com/UV%20SiC%20Avalanche%20Photodiodes.htm

[13] Kedar, D., & Arnon, S. (2006). Non-line-of-sight optical wireless sensor network operating in multiscattering channel. Applied Optics, 45(33), 8454.

[14] D. M. Reilly, D. T. Moriarty, and J. A. Maynard, “Unique properties of solar blind ultraviolet communication systems for unattended groundsensor networks,” in Unmanned/Unattended Sensors and Sensor Networks, E. M. Carapezza, Ed. SPIE, Nov. 2004.

[15] International Commission on Non-Ionizing Radiation Protection (ICNIRP): Guidelines on Limits of Exposure to Ultraviolet Radiation of Wavelengths between 180 nm and 400 nm (Incoherent Optical Radiation), republished in Health Physics, vol. 87, no. 2, 2004, pp. 171–86.

[16] G. Shaw, A.M.Siegel, and M.L.Nischan, \Demonstration system and applications for compact wireless ultraviolet communications," in AeroSense 2003, pp. 241{ 252, International Society for Optics and Photonics, 2003.

[17] Vavoulas, A., Sandalidis, H. G., Chatzidiamantis, N. D., Xu, Z., & Karagiannidis, G. K. (2019). A Survey on Ultraviolet C-Band (UV-C) Communications. IEEE Communications Surveys & Tutorials, 1–1.

[18] D. M. Reilly, “Atmospheric optical communications in the middle ultraviolet,” *M.S. Thesis*, MIT, Cambridge, MA, 1976

[19] D. M. Reilly and C. Warde, “Temporal characteristics of singlescatter radiation,” J. Opt. Soc. Am. 69, 464–470 (1979).

[20] M. R. Luettgen, D. M. Reilly, and J. H. Shapiro, “Non-line-of-sightsingle-scatter propagation model,” J. Opt. Soc. Am. A, vol. 8, no. 12, p. 1964, Dec. 1991.

[21] Ding, H., Chen, G., Xu, Z., & Sadler, B. M. (2012). Channel modelling and performance of non-line-of-sight ultraviolet scattering communications. IET Communications, 6(5), 514.

[22] M. A. Elshimy and S. Hranilovic, “Non-line-of-sight single-scatter propagation model for noncoplanar geometries,” J. Opt. Soc. Am. A, vol. 28, no. 3, p. 420, Feb. 2011.

[23] L. Wang, Z. Xu, and B. M. Sadler, “An approximate closed-form link loss model for non-line-of-sight ultraviolet communication in noncoplanar geometry,” Opt. Lett., vol. 36, no. 7, p. 1224, Mar. 2011.

[24] Y. Zuo, H. Xiao, W. Zhang, H. Xu, and J. Wu, “Approximate performance study of non-line-of-sight ultraviolet communication links in noncoplanar geometry,” in 7th International Conference on Communications and Networking in China. IEEE, Aug. 2012.

[25] H. Ding, G. Chen, A. Majumdar, B. Sadler, and Z. Xu, “Modeling of non-line-of-sight ultraviolet scattering channels for communication,” IEEE J. Sel. Areas Commun, vol. 27, no. 9, pp. 1535–1544, Dec. 2009

[26] Z. Xu, H. Ding, B. M. Sadler, and G. Chen, “Analytical performance study of solar blind non-line-of-sight ultraviolet short-range communication links,” Opt. Lett., vol. 33, no. 16, p. 1860, Aug. 2008.

[27] G. Chen, Z. Xu, H. Ding, and B. Sadler, “Path loss modeling and performance trade-off study for short-range non-line-of-sight ultraviolet communications,” Opt. Express, vol. 17, no. 5, p. 3929, Feb. 2009.

[28] R. J. Drost, T. J. Moore, and B. M. Sadler, “UV communications channel modeling incorporating multiple scattering interactions,” J. Opt. Soc. Am. A, vol. 28, no. 4, p. 686, Mar. 2011.

[29] Ding, H., Chen, G., Majumdar, A., Sadler, B., & Xu, Z. (2009). Modeling of non-line-of-sight ultraviolet scattering channels for communication. IEEE Journal on Selected Areas in Communications, 27(9), 1535–1544.

[30] Liu, W., Zou, D., & Xu, Z. (2015). Modeling of optical wireless scattering communication channels over broad spectra. Journal of the Optical Society of America A, 32(3), 486.

[31] M. H. Ardakani and M. Uysal, “Relay-assisted OFDM for ultraviolet communications: Performance analysis and optimization,” IEEE Trans. Wireless Commun, vol. 16, no. 1, pp. 607–618, Jan. 2017.

[32] M. H. Ardakani, A. R. Heidarpour, and M. Uysal, “Performance analysis of MIMO NLOS UV communications over atmospheric turbulence channels,” in 2016 IEEE Wireless Communications and Networking Conference Workshops (WCNCW). IEEE, Apr. 2016.

[33] ——, “Performance analysis of relay-assisted NLOS ultraviolet communications over turbulence channels,” IEEE J. Opt. Commun. Netw, vol. 9, no. 1, p. 109, Dec. 2016.

[34] Wang, L., Li, Y., & Xu, Z. On connectivity of wireless ultraviolet networks. Journal of the Optical Society of America A, 28(10), 2011.

[35] A. Vavoulas, H. G. Sandalidis, and D. Varoutas, “Connectivity issues for ultraviolet UV-c networks,” IEEE J. Opt. Commun. Netw, vol. 3, no. 3, p. 199, Feb. 2011.

[36] Wang, L., Li, Y., Xu, Z., & Sadler, B. M. (2010). Wireless ultraviolet network models and performance in noncoplanar geometry. In 2010 IEEE Globecom Workshops. IEEE.

[37] W. Fawaz, C. Abou-Rjeily, and C. Assi, “UAV-aided cooperation for FSO communication systems,” IEEE Commun. Mag, vol. 56, no. 1, pp. 70–75, Jan. 2018.

[38] A. Kaadan, H. Refai, and P. Lopresti, “Spherical FSO receivers for UAV communication: geometric coverage models,” IEEE Trans. Aerosp. Electron. Syst, vol. 52, no. 5, pp. 2157–2167, Oct. 2016

[39] T. Zhao, Y. Xie and Y. Zhang, "Connectivity properties for UAVs networks in wireless ultraviolet communication", Photonic Network Communications, vol. 35, no. 3, pp. 316-324, 2018.

[40] Xu, C., Zhang, H., & Cheng, J. Effects of haze particles and fog droplets on NLOS ultraviolet communication channels. Optics Express, 23(18), 2015.

[41] Ding, H., Xu, Z., & Sadler, B. (2010). A Path Loss Model for Non-Line-of-Sight Ultraviolet Multiple Scattering Channels. EURASIP Journal on Wireless Communications and Networking, 2010

[42] S. Navidpour, M. Uysal and M. Kavehrad, "BER Performance of Free-Space Optical Transmission with Spatial Diversity", IEEE Transactions on Wireless Communications, vol. 6, no. 8, pp. 2813-2819, 2007.

[43] Andrews, L. C., & Phillips, R. L. Laser Beam Propagation through Random Media. SPIE. 2005.

[44] Billingsley, P. Probability and Measure, Wiley-Interscience, 1995

VITA

Hamed Tadayyoni received his B.Sc. degree in electrical engineering from School of Electrical and Computer Engineering of University of Tehran, Iran. He is currently pursuing his M.Sc. studies at the department of Electrical and Electronics Engineering, Graduate School of Engineering, Ozyegin University, Istanbul, Turkey, as a research assistant in Communications Theory and Technology (CT&T) Lab, under supervision of Prof. Dr. Murat Uysal. His research interests include ultraviolet communications (physical layer theory and channel modeling).